ACS Catalysis

Perspective

pubs.acs.org/acscatalysis

Increasing Oxide Reducibility: The Role of Metal/Oxide Interfaces in the Formation of Oxygen Vacancies

Antonio Ruiz Puigdollers, Philomena Schlexer, Sergio Tosoni, and Gianfranco Pacchioni*

Dipartimento di Scienza dei Materiali, Università di Milano-Bicocca, via R. Cozzi, 55 I-20125 Milano, Italy

Supporting Information

ABSTRACT: Reducibility is an essential characteristic of oxide catalysts in oxidation reactions following the Mars–van Krevelen mechanism. A typical descriptor of the reducibility of an oxide is the cost of formation of an oxygen vacancy, which measures the tendency of the oxide to lose oxygen or to donate it to an adsorbed species with consequent change in the surface composition, from M_nO_m to M_nO_{m-x}. The oxide reducibility, however, can be modified in various ways: for instance, by doping and/or nanostructuring. In this review we consider an additional aspect, related to the formation of a metal/oxide interface. This can be realized when small metal nanoparticles are deposited on the surface of an oxide support or when a nanostructured oxide, either a nanoparticle or a thin film, is grown on a metal. In the past decade, both theory and experiment indicate a particularly high reactivity of the oxygen atoms at the boundary region between a metal and an oxide. Oxygen atoms can be removed from interface sites at much lower cost than in other regions of the surface. This can alter completely the reactivity of a solid catalyst. In this respect, reducibility of the bulk material may differ completely from that of the metal/oxide surface. The atomistic study of CO oxidation and water-gas shift reactions are used as examples to provide compelling evidence that the oxidation occurs at specific interface sites, the actual active sites in the complex catalyst. Combining oxide nanostructuring with metal/oxide interfaces opens promising perspectives to turn hardly reducible oxides into reactive materials in oxidation reactions based on the Mars–van Krevelen mechanism.

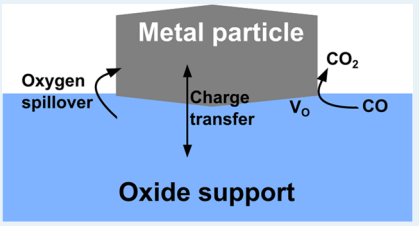

KEYWORDS: *oxide, reducibility, oxygen vacancy, density functional theory, CO oxidation, water-gas shift reaction*

1. INTRODUCTION: OXIDES IN HETEROGENEOUS CATALYSIS

Metal oxides are widely used in catalysis, as they represent essential components of an active heterogeneous catalyst. Searching the Web of Science for "oxides AND catalysis OR catalyst" provides about 300000 papers. Due to the huge variety of compositions and electronic and geometrical structures, metal oxides offer a very broad spectrum of properties and behaviors that can result in specific functionalities and chemical activities. Oxides can be used as "inert" supports of finely dispersed active metal nanoparticles or directly as catalysts. In this latter case, the oxide surface must be able to exchange chemical species with the liquid- or gas-phase surroundings or to adsorb chemical species and promote dissociation and regeneration of chemical bonds. The great flexibility of oxide surfaces stems from the presence on the surface of both Lewis and Brønsted acid and basic sites, sometimes acting in a cooperative way.[1]

Oxides can be divided into two main classes, depending on their chemical behavior: nonreducible and reducible oxides. Nonreducible oxides consist of materials that do not easily lose oxygen, due to the intrinsic resistance of the corresponding metal cations to change oxidation state. Since oxygen is formally in a −2 oxidation state, the excess electrons that are left on the material by removal of a neutral O atom cannot be accommodated in the cation empty states which lie too high in energy, contributing to the formation of the conduction band of the material. Oxides such as SiO_2, MgO, Al_2O_3, and many other main-group oxides belong to this class. Usually these materials are characterized by a very large band gap (typically >3 eV) separating the valence band (VB) from the conduction band (CB). The excess electrons left on the material when oxygen is removed in the form of O_2 or H_2O are trapped in specific sites (e.g., an oxygen vacancy) and give rise to new defect states in the band gap.[2] This process is energetically very costly, and therefore these as-prepared materials are highly stoichiometric, stable, and chemically inert.[3] The group of reducible oxides, in contrast, is characterized by the capability to exchange oxygen in a relatively easy way. This is because the lowest empty states available on the material (CB) consist of cation d orbitals which lie at not overly high energy with respect to the VB. These oxides usually have semiconductor character, with band gaps <3 eV. The removal of oxygen results in excess electrons that are redistributed on the cation empty levels, thus changing their oxidation state from M^{n+} to $M^{(n-1)+}$. Transition-metal oxides such as TiO_2, WO_3, NiO, Fe_2O_3, CeO_2, etc., just to mention a few, belong to this category.[4]

The difference between nonreducible and reducible oxides is of fundamental importance for the chemical reactivity of these materials. A substantial fraction of industrial catalysis is dealing

Received: June 12, 2017
Revised: August 15, 2017
Published: August 18, 2017

DOI: 10.1021/acscatal.7b01913
ACS Catal. 2017, 7, 6493−6513

with oxidation reactions or oxidative dehydrogenation processes. In most cases the active catalyst is an oxide, and the reaction follows a mechanism originally described by Mars and van Krevelen[5] and thus is named after the two authors (MvK). The key of the MvK mechanism is that the oxide surface is not just a spectator of the reaction but rather is directly involved via its most reactive oxygen atoms. An organic substance can react with these specific sites at the oxide surface (e.g., oxygen atoms located at low-coordinated sites). A weakly bound surface O atom is added to the reactant forming the oxygenated compound, leaving behind an oxygen vacancy on the surface, hereafter referred to as V_O. This results in a MO_{n-x} compound, with a stoichiometry which is no longer that of the starting MO_n oxide since oxygen has been lost in the process. In order to be catalytic, the reaction must occur under oxygen pressure so that molecular oxygen can interact with the surface, dissociate, and eventually refill the vacancy created in the oxidative process. In this way, the original stoichiometry and composition of the catalyst are restored, closing the catalytic cycle. Using isotopically labeled oxygen, it is possible to prove that the oxygen atom incorporated in the organic reactant does not come from the gas phase but rather is directly extracted from the solid surface.[6]

Clearly, in this kind of process a very good descriptor of the reaction is the cost of removing an oxygen atom from the clean surface of the catalyst. This in fact determines both the kinetics and the thermodynamics of the overall reaction. This simple example already shows that the generation of oxygen vacancies on the surface of an oxide is a very important aspect of its chemistry. The problem is that the identification and characterization of oxygen vacancies on oxide surfaces are far from trivial. In fact, one is dealing with the identification of a missing atom. For this reason, some years ago some of us discussed the role of oxygen vacancies on oxide surfaces as "the invisible agent on oxide surfaces".[7] In recent years several techniques have been developed to better identify and characterize these centers. Among others, scanning tunneling microscopy (STM) and atomic force microscopy (AFM) have progressively grown in importance for the atomistic characterization of these defects.[1,3,8,9] In particular, enormous progress has been made in the use of AFM which, at variance with STM, can be employed also on nonconducting supports. Since many oxides are insulating, in particular the nonreducible ones, this has opened the perspective to better characterize these centers on all forms of oxides, reducible and nonreducible. A combination of AFM and STM measurements can provide information on the localization and charge state of defects in oxides.[10,11]

A better knowledge of the nature and characteristics of anion vacancies on oxide surfaces is important because it allows the design of materials with tailored properties, in particular to prepare oxides that can be more or less reactive and that can (or cannot) exchange oxygen with adsorbed chemical species. This has prompted several researchers to explore methods or procedures to improve the reducibility of a metal oxide. In general, there are three main conceptual approaches to this target: (i) doping the material with heteroatoms, (ii) producing the oxide in form of nanocrystallites or thin films, and (iii) depositing metal nanoparticles on the surface of an oxide. All of these procedures are relatively novel, but probably, the importance of the last method, i.e. the formation of metal/oxide interfaces, has been fully realized only very recently. This is also the topic of this perspective article.

1.1. Oxide Reducibility: Effect of Doping. Doping oxides by heteroatoms and the effect on oxide reducibility have been studied recently both experimentally and theoretically with the hope of producing better catalytic materials, in particular for oxidation reactions.[12−14] The chemical, electrical, and optical properties of an oxide largely depend on the presence and the concentration of intrinsic or extrinsic defects. Defect engineering is the science that aims at manipulating the nature and the concentration of defects in a solid, as well as tuning its properties in a desired manner. For instance, defects can turn a colorless insulator into a black material with metallic conductivity or improve the photoactivity of an oxide semiconductor, making it able to absorb solar light.[15] In a similar way, one can modify the chemistry of an oxide surface by introducing heteroatoms in the structure.[14] One example is the substitution of a metal cation in an oxide of formula M_xO_y with another dopant, D. This results in a direct modification of the electronic structure of the oxide, with important consequences on its properties. If the doping heteroatom D has the same valence of the metal cation M that is replaced, then the modifications are restricted to size effects or, at most, to a shift of the frontier orbitals with consequent changes in the strength of the M−O and D−O bonds. Much more complex is the situation occurring when the dopant D has a different valence in comparison to the replaced cation. In this case, the simple substitution of the cation M results in a charge imbalance that needs to be compensated by the creation of other defects in the structure. The number of possibilities is extremely large, since in principle all atoms of the periodic table can be used to replace a metal cation in an oxide. The possibility to explore theoretically with first-principles simulations the effect of doping is thus of great help for the design of new catalytic materials. This problem has been extensively investigated and reviewed by Metiu and co-workers in a series of DFT calculations where several dopants have been introduced in an oxide matrix.[16] Both non-transition-metal and transition-metal atoms have been tested.[16] The general assumption is that any oxide modification that facilitates the removal of surface oxygen will facilitate the MvK mechanism in oxidation reactions. Since oxygen is electrophilic, one can expect to lower the cost to remove it from the surface by making the surface more electron deficient. This can be done, at least in principle, by replacing some of the cations of the host oxide with cation dopants D having a lower valence. Indeed, several theoretical studies indicate that the cost to create a V_O center near a low-valence dopant is lower than that on the undoped surface. It has also been observed that the presence of a low-valent dopant affects oxygen atoms several sites away from the dopants, with a relatively long-range effect. However, the easiest oxygen atom to remove remains that in direct contact with the dopant D. These conclusions appear to be rather general, as they have been obtained for several oxides, such as TiO_2, CeO_2, ZnO, La_2O_3, CaO, and NiO.[16]

The theoretical conclusions are supported by some experimental evidence that, indeed, doping improves the catalytic performances, by improving the conversion, the selectivity, or the surface area of the catalyst.

Oxide anions can also be replaced with direct effects on the properties of the material and in particular on its reducibility. A classic example is that of doping TiO_2 with nitrogen. Doping semiconductor oxides with nonmetal atoms has attracted huge interest in the last 15 years, in the attempt to improve the solar light absorption and to increase the generation of electron−

DOI: 10.1021/acscatal.7b01913
ACS Catal. 2017, 7, 6493−6513

hole pairs.[17−20] The N dopant can either replace an O atom in the lattice or take an interstitial position. In both cases, it introduces new defect states in the gap, just above the top of the valence band, thus lowering the energy required to excite an electron into the CB. An important secondary effect observed in N-doped titania is that the presence of partially filled N 2p states deep in the gap favors the formation of oxygen vacancies and hence the reducibility of the oxide.[19,20] The partially filled low-lying acceptor N 2p orbitals are able to trap the electrons released when an O atom is removed from the surface. The excess electrons, instead of being accommodated in the high-lying Ti empty 3d states ($Ti^{4+}(3d^0) + e^- \rightarrow Ti^{3+}(3d^1)$), close to the bottom of the CB, fill the low-lying singly occupied N 2p orbitals, with a large gain in stability. As a consequence, the cost to create a vacancy in bulk TiO_2 drops from 4.63 to 0.27 eV.[21] This effect is general and has been observed for many other oxides, including materials with high band gap and low reducibility such as ZrO_2[22] and MgO.[23] Thus, the presence of heteroatoms can have unexpected but profound consequences on the stability of the oxide and on its capability to release oxygen.

While conceptually very attractive, the idea to selectively dope an oxide material is difficult to realize in practice. The incorporation of heteroatoms, in fact, requires a specific chemical synthesis designed for this purpose, and the product has to be carefully characterized at an atomistic level to make sure that the preparation results in a doped material. This is far from simple. With a chemical synthesis, it is hard to know a priori the kind and concentration of dopants in the structure. This depends on the external conditions of temperature, pressure, purity of reactants, annealing, etc. Second, there is a large number of possible mechanisms for charge compensation, which opens a wide spectrum of combination of defects. For all these reasons, while doping with heteroatoms can significantly help the catalyst reducibility, our present understanding and control of the doping process for the rational design of new efficient and practical catalysts are still rudimentary.

1.2. Oxide Reducibility: Effect of Nanostructuring. Another way to improve oxide reducibility is to control the morphology and dimensionality of oxide particles. Oxygen ions at low-coordinated sites of an oxide surface can behave very differently from the corresponding bulk counterparts. One of the first oxides considered in this context was MgO.[24] MgO is an ionic oxide with a rock salt structure, a wide band gap, and very low chemical activity when it is prepared in single-crystal form. The (001) surface of MgO is notoriously inert and defect free. CO adsorption on a single crystal of MgO can only be realized at very low temperatures; in fact, the CO molecule is weakly bound by van der Waals forces to the surface and easily desorbs as the temperature exceeds 57 K.[25,26] Slightly higher desorption energies are measured for CO bound to Mg cations at steps and edges of the surface. Virtually no chemistry occurs on a single-crystal MgO surface. In contrast, if MgO nanocrystals are exposed to CO at 60 K, this results in a rich and complex chemistry, as shown, for instance, by a multitude of features due to the formation of carbonates and other $[O-CO]_n^{2-}$ species appearing in the infrared spectrum.[27−29] This is due to the much higher reactivity of the low-coordinated O sites at steps and corners, a result that has been fully rationalized in terms of the different Madelung potential at these sites in comparison to the regular MgO (001) surface.[30] In a similar way, generation of oxygen vacancies has a very different energy cost at the surface, where the cost is prohibitively high, and along steps and corners, where it decreases significantly.[24] Thus, oxide nanostructuring, which increases the ratio of surface versus bulk atoms, and in particular of the number of low-coordinated ions on the surface, can result in deeply modified properties of oxide materials.

The problem has been recently investigated for the case of ZrO_2. ZrO_2 is a highly ionic insulating oxide with a band gap of ∼6 eV;[31,32] it is considered a nonreducible oxide like MgO.[33] The removal of a O_{4c} ion from bulk has a energy cost of 6.16 eV. This is computed at DFT level with respect to $1/2O_2$, the standard reference for O vacancy formation energies. This reduces to 5.97 eV when a O_{3c} atom is removed from the (101) surface, a very small change (notice that the values of the V_O formation energy in ZrO_2 reported in this review may change by ±0.1 eV due to the different sizes of the adopted supercells). Instead, when ZrO_2 is nanoscaled down to nanoparticles of 1−2 nm size, the formation energy of an O vacancy is significantly lower. For instance, removing a corner O_{2c} atom from the $Zr_{16}O_{32}$, $Zr_{40}O_{80}$, and $Zr_{80}O_{160}$ nanoparticles has energy costs of 3.94, 3.70, and 2.26 eV, respectively; 4−5 eV is required to remove O_{3c} atoms at facets of the nanoparticles.[34,35] The O_{2c} and O_{3c} sites in the nanoparticles become important catalytic centers in reactions involving oxygen transfer. The possibility of modifying the reducibility of zirconia may have important implications in catalysis. For example, prereduced solid catalysts based on ZrO_2 nanoparticles display a better activity in the transformation of biomass into fuels.[36,37] In addition, reduced ZrO_{2-x} is shown to be photocatalytically active in H_2 production under solar light while stoichiometric ZrO_2 is inactive.[38]

A similar response has been found for CeO_2. Differently from zirconia, CeO_2 is a reducible oxide, whose catalytic activity is closely related to the change from +4 to +3 in the oxidation state of the cerium cations and its capacity to release oxygen according to the reaction $2CeO_2 \rightarrow Ce_2O_3 + 1/2O_2$.[39] The energy required to create a O_{4c} vacancy in bulk CeO_2 is 4.73 eV;[40] this reduces to 2.25 eV on the (111) surface (O_{3c}).[41,42] However, when $Ce_{21}O_{42}$, $Ce_{40}O_{80}$, and $Ce_{80}O_{160}$ nanoparticles are considered, the formation energies of a corner O_{2c} vacancy decrease to 1.67, 0.80, and 1.20 eV, respectively.[43] The enhanced reducibility at the nanoscale is observed also when a metal cluster is deposited on a CeO_2 nanoparticle. It has been demonstrated, both by experiment and by DFT calculations, that O spillover occurs spontaneously at room temperature from the supporting CeO_2 nanoparticle to a deposited Pt cluster, while on the extended CeO_2 surface this process is highly endothermic (this topic will be reconsidered below, at the end of this Perspective).[41,42] Thus, CeO_2 nanoparticles can dramatically improve the catalytic activity in comparison to bulk ceria.

Therefore, as for ZrO_2, also for CeO_2 the redox behavior changes dramatically at the nanoscale, where formation of V_O centers becomes easier. A deep understanding of these phenomena is essential for the use of these oxides in catalysis.[44] The phenomenon can be rationalized in two ways. First, nanoparticles contain a large fraction of undercoordinated cations such as corners and edges, whose empty d or f states are stabilized with respect to the bottom of the CB. Thus, empty M_{nd} defective electronic states are introduced in the band gap that lower the energy cost to accommodate the extra charge associated with an O vacancy.[34,35] Consequently, the electron density of the reduced system tends to be localized in low-

DOI: 10.1021/acscatal.7b01913
ACS Catal. 2017, 7, 6493−6513

Table 1. Overview of Direct Experimental Evidence That the Presence of a Metal Facilitates the Formation of Oxygen Vacancies on an Oxide Surface

year	ref	title	exptl methods used[a] and short description
2016	60	Formation and removal of active oxygen species for the noncatalytic CO oxidation on Au/TiO_2 catalysts	TAP, TPD distinction between noncatalytic "irreversible" oxygen species and catalytically active "reversible" oxygen species for the CO oxidation reaction over Au/TiO_2, the latter being titania lattice oxygen
2016	61	How temperature affects the mechanism of CO oxidation on Au/TiO_2: a combined EPR and TAP reactor study of the reactive removal of TiO_2 surface lattice oxygen in Au/TiO_2 by CO	EPR, TAP removal of TiO_2 surface lattice oxygen from a Au/TiO_2 catalyst and Ti^{3+} formation upon exposure to CO
2016	62	Mild activation of CeO_2-supported gold nanoclusters and insight into the catalytic behavior in CO oxidation	TAP redox cycle in which CO could reduce the surface of CeO_2 to produce oxygen vacancies active oxygen species present on the surface of the pretreated catalyst react with CO pulses to generate CO_2
2016	63	Direct evidence for the participation of oxygen vacancies in the oxidation of CO over ceria- supported gold catalysts by using operando Raman spectroscopy	operando Raman, IR direct spectroscopic evidence for the participation of oxygen vacancies in the oxidation of CO over ceria-supported gold
2016	64	Catalytic oxidation of carbon monoxide over of gold-supported iron oxide catalyst	FTIR, TEM, XRD the reducibility of the support is greatly enhanced and shifted to lower temperatures; this shift is due to strong interaction between the support and Au nanoparticles
2015	65	An atomic-scale view of CO and H_2 oxidation on a Pt/Fe_3O_4 model catalyst	STM CO extracts lattice oxygen atoms at the cluster perimeter to form CO_2, creating large holes in the metal oxide surface
2015	66	High activity of Au/γ-Fe_2O_3 for CO oxidation: effect of support crystal phase in catalyst design	CO-TPR, sequential pulse reaction, in situ Raman spectroscopy Au/γ-Fe_2O_3 shows higher activity for CO oxidation than Au/α-Fe_2O_3 systematic study shows that this higher-redox-property-based higher activity could be extended to γ-Fe_2O_3-supported Pt-group metals and to other reactions that follow Mars–Van Krevelen mechanism
2014	67	On the origin of the selectivity in the preferential CO oxidation on Au/TiO_2—Nature of the active oxygen species for H_2 oxidation	TAP absolute amount of active oxygen for H_2 oxidation is identical to that in CO oxidation, and is positioned at the Au/TiO_2 interface perimeter.
2013	68	Origin of the high activity of Au/FeO_x for low-temperature CO oxidation: Direct evidence for a redox mechanism	FTIR, Raman spectroscopy, microcalorimetry, DFT unambiguous evidence that the surface lattice oxygen of the FeO_x support participates directly in the low-temperature CO oxidation verification via DFT: oxygen vacancy formation at Pt_{8-10}/FeO_x perimeter
2013	69	Generation of oxygen vacancies at a Au/TiO_2 perimeter interface during CO oxidation detected by in situ electrical conductance measurement	in situ ECM detection of Ti^{3+} formation under reaction conditions for CO oxidation with O_2 over Au/TiO_2 catalyst
2011	70	Active oxygen on a Au/TiO_2 catalyst: Formation, stability, and CO oxidation activity	TAP correlation between oxygen storage capacity and CO oxidation activity results allow clear identification of the nature of the active oxygen species and their location on the catalyst surface
2011	41	Support nanostructure boosts oxygen transfer to catalytically active platinum nanoparticles	RPES and DFT electron transfer from the Pt nanoparticle to the support and oxygen transfer from ceria to the Pt nanoparticle. oxygen transfer is shown to require the presence of nanostructured ceria in close contact with Pt.
2010	71	Support effects in the Au-catalyzed CO oxidation—Correlation between activity, oxygen storage capacity, and support reducibility	TAP four different metal oxide supported Au catalysts with similar Au loading and Au particle sizes (Au/Al_2O_3, Au/TiO_2, Au/ZnO, Au/ZrO_2) are compared

DOI: 10.1021/acscatal.7b01913
ACS Catal. 2017, 7, 6493−6513

Table 1. continued

year	ref	title	exptl methods used[a] and short description
			oxygen storage capacity and activity for CO oxidation differ significantly for these catalysts and are correlated with each other and with the reducibility of the respective support material, pointing to a distinct support effect and a direct participation of the support in the reaction
2010	72	The interplay between structure and CO oxidation catalysis on metal−supported ultrathin oxide films	STM, AES, TDS, LEED, DFT oxygen enrichment of FeO/Pt(111) to FeO_x/Pt(111) (with $x \rightarrow 2$) and subsequent CO oxidation via the Mars−van Krevelen mechanism
2009	73	Reactive oxygen on a Au/TiO_2 supported catalyst	TAP both the oxygen storage capacity and the activity for CO oxidation scale linearly with the Au/TiO_2 perimeter length
2009	74	Kinetic and mechanistic studies of the water-gas shift reaction on Pt/TiO_2 catalyst	SSITKA, DRIFTS redox mechanism demonstrated as the prevailing mechanism on a Pt/TiO_2 catalyst, where labile oxygen and oxygen vacancies of TiO_2 near the metal−support interface can participate in the reaction path of the water-gas shift reaction
2007	75	Activation of a Au/CeO_2 catalyst for the CO oxidation reaction by surface oxygen removal/oxygen vacancy formation	TAP first experimental verification of a CO oxidation rate enhancement by oxygen surface vacancies on a realistic oxide-supported Au catalyst
2004	76	Nanocrystalline CeO_2 increases the activity of Au for CO oxidation by 2 orders of magnitude	TEM, IR, XPS, GC formation of Ce^{3+} under exposure of the catalyst to CO at 60 °C
2004	77	Strain-induced formation of arrays of catalytically active sites at the metal-oxide interface	STM, DFT annealing under vacuum leads to the formation of a CeO_{2-x} phase, as indicated by the transformation of Ce^{4+} into Ce^{3+} species metal−oxide interface creates preferential sites for the reduction of the ceria
2004	78	CO spillover and oxidation on Pt/TiO_2	TPD observation of CO_2 production upon exposure of the Pt/TiO_2 catalyst to CO, even without supply of O_2 in the gas mixture

[a]Acronyms: AES = Auger electron spectroscopy, CO-TPR = temperature-programmed reduction with CO, DFT = density functional theory, DRIFTS = diffuse reflectance infrared Fourier transform spectroscopy, ECM = electrical conductance measurement, EPR = electron paramagnetic resonance, (FT)IR = (Fourier transform) infrared spectroscopy, GC = gas chromatography, LEED = low-energy electron diffraction, RPES = resonant photoelectron spectroscopy, SSITKA = steady-state isotopic transient kinetic analysis, STM = scanning tunneling microscopy, TAP = temporal analysis of products, TDS = thermal desorption spectroscopy, TPD = temperature-programmed desorption, XPS = X-ray photoelectron spectroscopy, XRD = X-ray diffraction.

DOI: 10.1021/acscatal.7b01913
ACS Catal. 2017, 7, 6493−6513

coordinated Zr^{3+} and Ce^{3+} centers that, trapping a single electron, become magnetic and can be detected by electron paramagnetic resonance (EPR).[34,35,40,33,45,46] The second aspect is the increased structural flexibility. Nanoparticles and in general nanostructures are more flexible than extended surfaces or the bulk material.[47] Atomic relaxation around the created O vacancy occurs at much lower cost, thus contributing to stabilize the defect.[34,35,45] In short, both the size and morphology of oxide supports are very important in determining the catalytic processes.

1.3. Oxide Reducibility: Effect of Metal/Oxide Interface. The interface between an oxide surface and a metal is of crucial importance in several modern technologies. Metal/oxide interfaces find application in microelectronic devices to create Schottky contacts and metal/oxide resistive random access memories, in electrochemistry for contact electrodes, in corrosion protection as oxide films to form a protective barrier against the oxidation of the underlying metal, in catalysis for supported metal nanoparticles, etc. Despite the technological importance of metal/oxide interfaces, our knowledge of the interface between a metal and an oxide is still very unsatisfactory. The reason is that the interface is difficult to access experimentally with the typical techniques available in surface science and is also difficult to describe theoretically, as it involves two materials with completely different properties: a conductive metal on one side and an insulator or semiconductor phase on the other. DFT has problems in treating on an equal footing these two classes of materials: methods that work very well for one category (e.g., standard GGA functionals for metals) usually perform poorly for the second component (the insulating phase); vice versa, self-interaction corrected functionals work well for semiconductors and insulators but may fail when it comes to describing a metallic phase.[48]

Despite these problems, it is becoming increasingly clear that the contact region between an oxide and a metal is chemically very active. One aspect of key importance is the occurrence of a direct charge transfer between the metal and the oxide.[49] Metals with low work function deposited on oxides with high electron affinity can induce the reduction of the oxide by direct electron transfer. The oxide surface becomes electron rich and thus changes its chemical properties. Of course, oxygen exchange can be affected by this phenomenon as well, although this has not been studied in detail until very recently.

The interface between a metal and an oxide is strongly affected by the presence of oxygen vacancies. So far, most of the attention has been dedicated to the fact that vacancies, when present, play an important role in stabilizing deposited metal nanoparticles and eventually in tuning their chemical activity.[50−56] Theory has shown that metal atoms and clusters bind much more strongly to these defect sites. New experiments have been designed to nucleate clusters under controlled conditions or even to deposit via soft-landing techniques mass-selected clusters generated in the gas phase.[57] These experiments offer a unique opportunity to study the cluster reactivity as a function of the particle size and of the deposition site,[56,58,59] opening new perspectives for the understanding of the basic principles of catalysis by small metal particles. For very small cluster sizes, in the nanometer size regime, the strong interaction with a surface defect may lead to a modification of the chemical activity of the particle.[50,51,56] The literature about the role of surface oxygen vacancies in promoting nucleation and growth of deposited metal atoms and clusters is very abundant and covers several oxides and virtually every metal.

What has attracted much less attention, however, is the fact that by depositing a metal cluster on an oxide surface one may also favor the formation of oxygen vacancies. The idea is that the metal/oxide interface, in particular the periphery between a metal nanoparticle and the oxide support, are regions where the oxide reactivity is significantly enhanced and where oxygen can be easily removed. This is also the main topic of this review. By considering a number of examples, from both theory and experiment, we will demonstrate that the reducibility of an oxide can be deeply modified by creating contacts between metals and oxide surfaces. Table 1 reports a noncomprehensive overview of direct experimental evidence that the presence of a metal facilitates the formation of oxygen vacancies on oxide surfaces.[60−78] This will be further commented upon in the next sections.

2. METAL/OXIDE INTERFACE AND OXIDE REDUCIBILITY

2.1. Theory of Metal Clusters on Oxide Surfaces: V_O Formation Energies. Likely, the first indication that oxygen vacancies can form at lower cost when a metal is in contact with an oxide surface came from theory. About 20 years ago it became possible, thanks to continuous advances in computer power and to the development of accurate functionals for DFT calculations, to study systems of increasing complexity, including cases of small metal clusters supported on oxide surfaces or even of extended metal/oxide interfaces. As we mentioned above, it was immediately realized that, in the presence of surface oxygen vacancies, the adhesion energy of the metal increases, and consequently the tendency of the supported particles to diffuse and aggregate decreases. However, it was only about 15 years ago that it was reported explicitly that the role of the metal could also be that to reduce the cost to create an oxygen vacancy, thus favoring the reduction of the oxide. A DFT study of the Pd/MgO interface reported that the formation energy of V_O at the Pd/MgO interface, 8.4 eV, is about 1 eV smaller than that on the regular surface, where it is 9.5 eV (these values are referenced to a gas-phase O atom).[79,80] The difference is modest but relevant, and the effect was attributed to the stabilizing effect of the metal when the vacancy is formed.

The topic was then reconsidered shortly after by Honkala and Hakkinen, who found on studying Au clusters deposited on the MgO(001) surface that the formation of an interfacial V_O defect center is thermodynamically more favorable than the formation of a surface vacancy.[81] These studies, however, were dealing with a nonreducible oxide, MgO, and were not directly supported by experimental evidence. Furthermore, even a reduction of about 1 eV out of formation energy close to 10 eV is not going to significantly change the landscape of the MgO surface chemistry. Thus, it is not surprising that these findings did not attract particular attention.

Things changed shortly thereafter, when it started to emerge that the role of supported metal nanoparticles could be significant in the context of the reducibility of semiconductor oxides. The effect of metal clusters on the reducibility of TiO_2 was explicitly discussed in a DFT study by Cheettu and Heyden.[82] They used both cluster and slab models with standard (PBE) and hybrid (PBE0) functionals to investigate the influence of Au and Pd dimers and trimers on the cost to remove an O atom from the TiO_2(110) rutile surface. The

DOI: 10.1021/acscatal.7b01913
ACS Catal. 2017, 7, 6493−6513

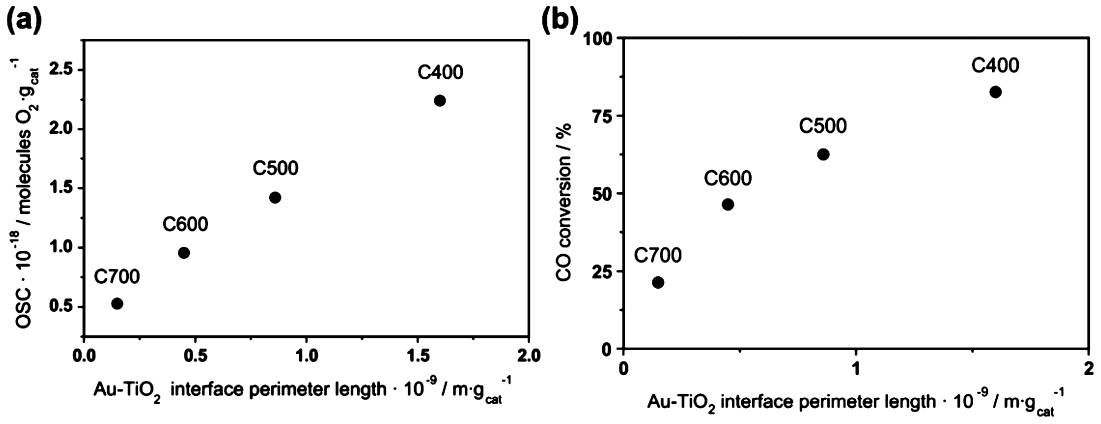

Figure 1. (a) Oxygen storage capacity of the Au/TiO_2 catalysts in multipulse experiments at 80 °C after different calcination pretreatments (400, 500, 600, and 700 °C). (b) Relative conversion of CO at 80 °C of the same catalysts during simultaneous CO/Ar and O_2/Ar pulses. Reprinted with permission from ref 73. Copyright 2009 Elsevier Ltd.

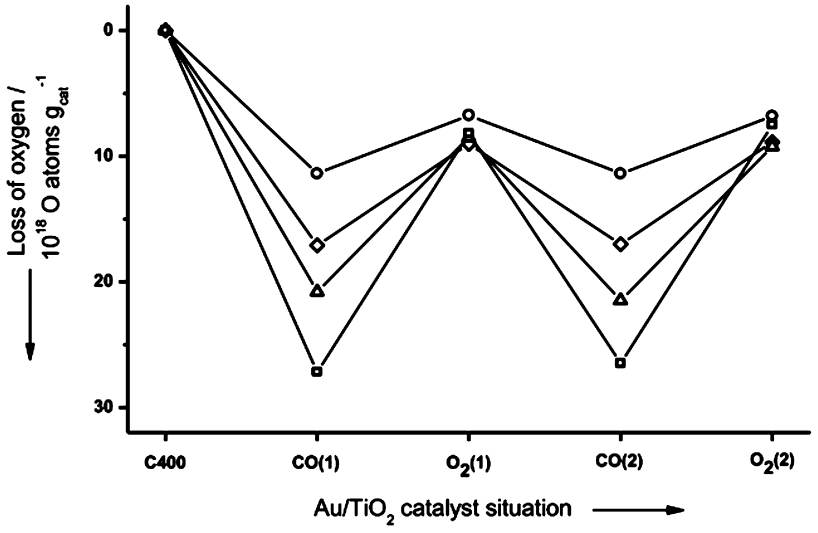

Figure 2. Loss of oxygen referenced to the oxygen content after oxidative pretreatment (C400), after reduction by CO/Ar pulses (CO(1)), after reoxidation by O_2 /Ar pulses (O_2(1)), and after second sequences of CO (CO(2)) and O_2 (O_2(2)) pulses at different temperatures: 80 °C (○); 160 °C (◇); 240 °C (△); 400 °C (□). Reprinted with permission from ref 90. Copyright 2014 American Chemical Society.

calculations showed a substantial effect. The formation energy of a V_O center on rutile was found to be 3.75 eV (PBE) or 4.37 eV (PBE0); these values are slightly reduced in the presence of Au clusters and strongly reduced by the presence of Pt clusters. In particular, a Pt dimer lowers the formation energy of the vacancy to 2.12 eV (PBE) or 2.10 eV (PBE0), i.e. by about 1.6−2.3 eV, depending on the method adopted.

Further evidence came from some key experiments that showed unambiguously the role of lattice oxygen in oxidation reactions catalyzed by supported metal particles. We are referring in particular to the case of CO oxidation over gold particles supported on TiO_2.

2.2. CO Oxidation on Au/TiO_2. Probably, CO oxidation over supported gold nanoparticles is one of the most studied reactions in catalysis. Searching for "CO oxidation" in the ISI WoS gives 14000 papers, which are reduced to about 1000 if the search is restricted to "CO oxidation AND Au/TiO_2". Despite the large number of studies, the mechanism of CO oxidation on Au/TiO_2 is still a matter of debate. Several mechanisms have been proposed, but clearly different reaction paths are followed at different temperatures. In the so-called low-temperature regime, it is assumed that both CO and O_2 molecules from the gas phase adsorb on the metal particle, with O_2 bound at the interface between gold and the oxide support.[83−87] The bond of the O_2 molecule is weakened by the interaction with the solid surface. CO can react and bind an O atom of the activated O_2 molecule to form CO_2 and an adsorbed O adatom, overcoming a low barrier. A second CO molecule binds to the Au catalyst and reacts with the O adatom to form CO_2. There are several pieces of evidence that this is the mechanism, and it has been shown that an excess of negative charge on the Au cluster, due for instance to the presence of an oxygen vacancy, can result in the formation of the more reactive superoxo O_2^- species, which is paramagnetic and has a characteristic EPR signal.[83] This mechanism is of Langmuir−Hinshelwood (LH) type and requires that both CO and O_2 can stick to the surface, diffuse, and react while bound to the catalyst. However, O_2 binds only weakly to Au: it desorbs from Au surfaces for $T > 170$ K.[88] Thus, this mechanism cannot work at room or higher temperatures since there is no adsorbed oxygen under these conditions.

This prompted some groups to propose a different mechanism, of MvK type, where the active species is the titania lattice oxygen. On the basis of kinetic measurements and

DOI: 10.1021/acscatal.7b01913
ACS Catal. 2017, 7, 6493−6513

temporal analysis of products (TAP) reactor measurements, Kotobuki et al.[73] demonstrated that both the oxygen storage capacity (OSC) of Au/TiO_2 catalysts and the catalytic activity for CO oxidation scale linearly with the Au/TiO_2 perimeter length. OSC is the amount of O_2 that can be stored on the catalyst surface. The Au/TiO_2 catalysts were prepared with equal Au loading but different Au mean diameters, obtained by different calcination pretreatments at 400, 500, 600, and 700 °C (denoted as C400, C500, C600, and C700, respectively). The treatments resulted in Au particle mean diameters of 3.5 ± 0.9, 4.8 ± 1.0, 6.7 ± 1.5, and 11.6 ± 3.1 nm. Exposing the catalysts to CO pulses at 80 °C results in CO_2 formation, although no O_2 was supplied in the gas mixture, indicating an effective reduction of the catalyst. Upon exposure of the reduced catalyst to O_2 pulses (still at 80 °C), a part of the oxygen remained on the catalyst, indicating its reoxidation. The reduction and the reoxidation are completely reversible, except for the first exposure to CO.

The OSCs of the different catalyst samples are shown in Figure 1a. A linear dependence of the OSC on the Au/TiO_2 perimeter length can be observed. Figure 1b shows the relative CO conversion under steady-state conditions of the catalysts under simultaneous exposure to CO and O_2. Again, a roughly linear dependence of the relative CO conversion and the Au/TiO_2 perimeter length can be observed. These findings clearly indicate that the Au/TiO_2 perimeter sites are the active sites under the reaction conditions applied. However, no further specification of the exact nature of the oxygen species stored at the Au/TiO_2 perimeter can be deduced from these experiments.[73]

Widmann et al.[89] compared the OSCs and catalytic activities of Au nanoparticles supported on different oxides under identical conditions and found that they differ significantly for different catalyst types. Both the OSC and the catalytic activity correlate with the oxide reducibility, indicating a direct participation of the support in the reaction. Widmann et al.[70] also established the nature of the active oxygen species on the basis of multipulse measurements performed in a TAP reactor at temperatures between 80 and 400 °C. Upon sequential exposure to CO and O_2 pulses, they observed the reversible removal and replenishment of oxygen species of the catalyst, whereby the amount of oxygen removed from the catalyst increased with increasing temperature, as shown in Figure 2.

The temperature dependence of the amount of oxygen removed from the catalyst indicates that the catalyst reduction is an activated process (Figure 2). The high stability of the active oxygen species speaks against molecularly adsorbed oxygen. Furthermore, the fact that the oxygen removed increases with the temperature, but not the total amount of active oxygen after reoxidation, is a clear indicator that the active oxygen is lattice oxygen from the supporting TiO_2. This implies that CO abstracts a TiO_2 lattice oxygen at the Au/TiO_2 perimeter with creation of an oxygen vacancy, which is then refilled in the subsequent exposure to O_2. This reaction pathway corresponds to a Au-assisted MvK mechanism.[90] Note that no reaction occurs without the Au nanoparticles.

Further evidence for the formation of oxygen vacancies were provided by Maeda et al.,[69] who performed in situ electrical conductance measurements showing a sharp increase of the electrical conductance of the Au/TiO_2 catalyst upon exposure to the CO/O_2 reactant mixture. The method is highly sensitive toward detection of oxygen vacancies in TiO_2, as these centers are responsible for the generation of conducting electrons. In another experiment, Widmann et al.[61] detected the formation of Ti^{3+} species under exposure of a Au/TiO_2 catalyst to CO in a combined EPR and TAP reactor study. They showed that CO oxidation via the Au-assisted MvK mechanism takes readily place at 120 °C and is still possible at −20 °C, although with a slower kinetics. The formation of oxygen vacancies via abstraction by CO is then completely inhibited at −90 °C. Thus, at low temperatures, an LH type mechanism is proposed to be the dominant reaction pathway.

The feasibility of the MvK mechanism for CO oxidation over Au/TiO_2 has been studied and also confirmed computationally. Li et al.[91] performed Born−Oppenheimer molecular dynamics (BOMD) simulations of the CO oxidation reaction over Au_{16} and Au_{18} clusters supported on the titania rutile (110) surface. They found that CO adsorbed at the Au_{16}/TiO_2 perimeter prefers the removal of a titania lattice oxygen instead of an O_2 molecule adsorbed at a close-by dual perimeter site, as shown in Figure 3.

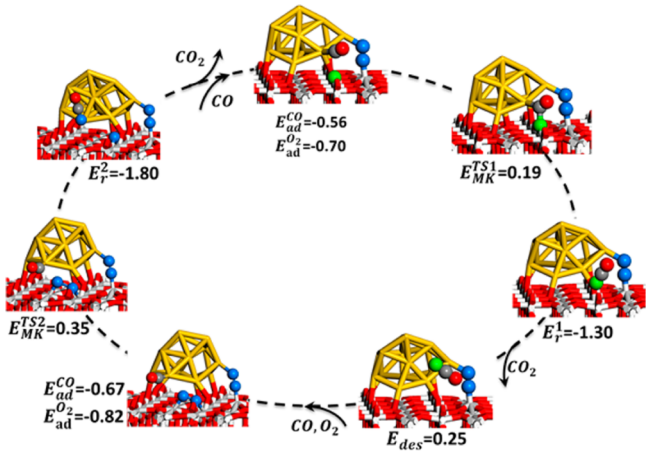

Figure 3. Reaction pathway for CO oxidation at Au_{16}/TiO_2 interface, following the Au-assisted MvK mechanism. E_{ad} (eV) represents adsorption energy and E^{TS} (eV) represents the reaction barrier for the generation and refilling of the oxygen vacancy. Negative and positive values indicate exothermic and endothermic processes, respectively. Reprinted with permission from ref 91. Copyright 2014 American Chemical Society.

The activation barrier for the oxygen removal from the titania lattice was as small as 0.19 eV in this case (Figure 3). The replenishment of the oxygen vacancy by O_2 exhibited a barrier of 0.35 eV. On the other hand, the alternative LH mechanism including the formation of a OCOO species exhibited an activation barrier of 0.62 eV. For the Au_{18} cluster, the reaction barriers for both reaction mechanisms were quite low as well (below 0.5 eV). In this case, however, the LH mechanism exhibited lower barriers than the MvK mechanism. Here, the LH mechanism was also the observed reaction pathway in the BOMD simulations. This difference between Au_{16} and the Au_{18} clusters was attributed to the larger fluxionality of Au_{16}.[92] Furthermore, a relation between the O_2 binding strength at the Au/TiO_2 interface and the energy required to remove a lattice oxygen from the support has been proposed: the stronger the O_2 molecules bind to the dual perimeter sites, the easier is to extract the lattice oxygen.

In a DFT+U study employing a Au rod supported on the titania rutile (110) surface, Duan et al.[93] obtained a similar picture considering the cost to create an oxygen vacancy upon

DOI: 10.1021/acscatal.7b01913
ACS Catal. 2017, 7, 6493−6513

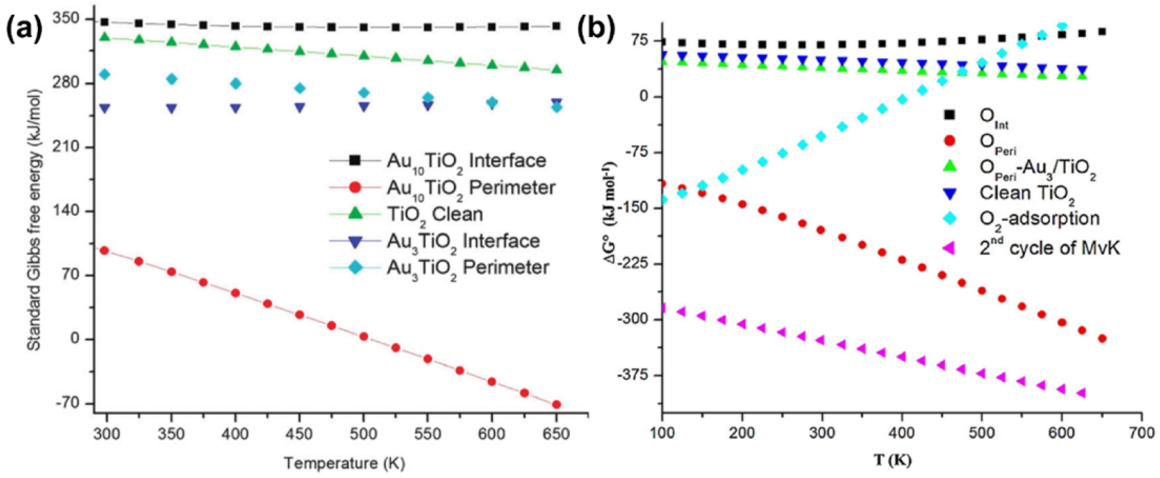

Figure 4. (a) Standard Gibbs free energy change for the formation of an oxygen vacancy $\Delta G^\circ(V_O)$ for different systems and V_O positions. (b) ΔG° for the formation of different intermediates on the model systems. O_{Int} and O_{Peri} show ΔG° for CO_2 formation on Au_{10}/TiO_2 using interface and perimeter oxygen atoms, respectively. O_{Peri}-Au_3/TiO_2 and clean TiO_2 show CO oxidation using O_{Peri} of Au_3/TiO_2 and lattice oxygen of clean TiO_2 surface, respectively. O_2 adsorption and the second cycle of MvK represent the adsorption of O_2 on the perimeter vacancy and CO oxidation by atomic oxygen on the Au_{10}/TiO_2 catalyst, respectively. Reprinted with permission from (a) ref 94, copyright 2015 Royal Society of Chemistry, and (b) ref 95, copyright 2016 Elsevier Ltd.

formation of atomically adsorbed oxygen at the Au/TiO_2 interface. They found a barrier of only 0.24 eV for CO oxidation via the LH mechanism, whereas the removal of lattice oxygen by CO was found to exhibit a barrier of 0.55 eV. The role of oxygen adatoms at the Au/TiO_2 interface is thereby to act as an electron acceptor, retrieving the excess electrons associated with the formation of an oxygen vacancy.

In two sequential DFT+U studies, Saqlain et al.[94,95] investigated the thermal activation of lattice oxygen on the TiO_2 anatase (001) surface with and without Au clusters. They observed a clear decrease in the oxygen vacancy formation free energy, $\Delta G^\circ(V_O)$, at Au_{10}/TiO_2 perimeter sites with respect to the Au-free titania surface (Figure 4a). They also established that, at these Au_{10}/TiO_2 sites, $\Delta G^\circ(V_O)$ becomes negative for $T > 230$ °C, the temperature at which the formation of oxygen vacancies becomes exergonic (Figure 4a). Then, they investigated CO oxidation with a titania lattice oxygen via the MvK mechanism. In agreement with the trend observed for the oxygen vacancy formation energies (Figure 4a), CO oxidation with a lattice oxygen at the Au_{10}/TiO_2 perimeter sites is favorable even at very low temperatures (Figure 4b). The activation barrier for the removal of lattice oxygen is 0.55 eV, according to this study. The barriers involved in the reoxidation process were below 0.4 eV. The observed difference between the Au_3 and the Au_{10} clusters in stabilizing the oxygen vacancies has been explained by the fact that Au_{10} can capture more electron density from the vacancy.

In a study based on ab initio molecular dynamics simulations (AIMD) and microkinetic modeling, Wang et al.[96] proposed a single gold atom MvK and hybrid single atom/nanoparticle mechanisms at the interface between a Au_{20} cluster and the titania rutile (110) surface. In this mechanism, a stable O_{ad}–Au^+ species forms and adsorbs CO, resulting in an O_{ad}–Au–CO species in proximity to the Au particle. Under highly oxidizing conditions, the Au_{20}/TiO_2 perimeter can be oxidized via formation of oxygen adatoms at dual perimeter sites. This facilitates the abstraction of a vicinal lattice oxygen by CO (of the O_{ad}–Au–CO species).

Although the findings of the various computational studies differ in their details, there are some recurring motifs, such as the role of the Au particles in stabilizing the oxygen vacancies by electron capture and an intimate interaction of a Au atom with the vacancy. The latter aspect is clearly related to the particle fluxionality, since rigid clusters are less capable of establishing a close interaction with the vacancy. Molecular and atomic oxygen at dual Au/TiO_2 perimeter sites enhance the electron affinity of the supported Au clusters and therefore increase their ability to stabilize oxygen vacancies by capturing excess charge. The adsorption energies reported for molecular O_2 adsorption at the cluster/surface perimeter are strongly dependent on the oxidation state of the ions in this region.

Under highly oxidizing conditions, O_2 molecules adsorb only weakly at the Au/TiO_2 perimeter and should therefore desorb at high temperatures. Most important, the computational studies demonstrate the feasibility of CO oxidation with the titania lattice oxygen thanks to relatively small activation barriers. Thus, the experimental findings that the Au-assisted MvK mechanism is the dominating reaction pathway under dry reaction conditions and at "elevated" temperatures ($T > 80$ °C) is clearly supported by theoretical studies.

2.3. CO Oxidation: Not Only Au on TiO_2. In this section, we discuss other cases of CO oxidation reactions with direct involvement of lattice oxygen at the metal/oxide interface, beyond Au/TiO_2. Diebold, Parkinson, and co-workers performed an STM study[65] of a catalyst consisting of Pt on Fe_3O_4 in CO and H_2 oxidation. Pt nanoclusters of size from one to six metal atoms were obtained from deposition of Pt atoms on a $Fe_3O_4(001)$ surface. Exposure of the sample to CO, O_2, and H_2 at room temperature did not produce any observable change in the STM images of the supported species. However, CO exposure at 550 K resulted in large holes covering about 3.7% of the surface and associated with at least one Pt cluster (Figure 5).

None of the morphological changes observed occurs in the absence of the Pt clusters, and DFT+U calculations provided evidence that the O atoms near the Pt/oxide interface are easier to remove. When the Pt/Fe_3O_4 model catalyst is exposed to O_2

DOI: 10.1021/acscatal.7b01913
ACS Catal. 2017, 7, 6493–6513

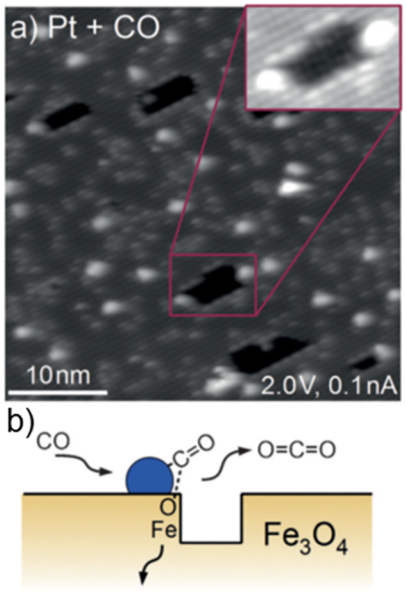

Figure 5. (a) STM images acquired following exposure of the Pt/Fe_3O_4(001) model catalyst to 1 × 10^{-7} mbar of CO at 550 K. Approximately 50% of the Pt clusters sit at the edge of or inside monolayer holes in the Fe_3O_4(001) terrace. (b) Illustration showing how CO extracts lattice O atoms from the cluster perimeter and how CO_2 desorbs from the surface. Undercoordinated Fe atoms diffuse into the Fe_3O_4 bulk. Reprinted with permission from ref 65. Copyright 2015 John Wiley and Sons.

at 550 K, the Pt clusters catalyze the growth of a new stoichiometric Fe_3O_4(001) surface. The work[65] provides clear evidence that the reduction and reoxidation of the Fe_3O_4 support are catalyzed by the Pt clusters.

The role of the metal/oxide interface in promoting CO oxidation has also been confirmed by recently reported DFT calculations on Au/CeO_2. Kim and Henkelman considered the reaction on Au_{12} nanoclusters supported on the regular and stepped CeO_2(111) surface, finding[97] an MvK type of mechanism mediated by lattice oxygen; the same role for the CeO_2 lattice oxygen was found experimentally by Li et al. at the boundaries of thiolate-capped Au_{144} clusters.[98] Hoh et al. studied the effect of Au nanoparticles supported on a Fe_2O_3(001) surface on the V_O formation energy, showing a substantial lowering to 2.13 eV near the cluster, while the cost for the bare surface is of 3.04 eV (computed with respect to 1/$2O_2$).[99]

Quite interestingly, the CO oxidation reaction can also occur via a MvK mechanism on a nonreducible oxide such as ZrO_2, provided that gold nanoparticles are deposited on it.[100] Using a DFT approach, it has been found that Au/ZrO_2 can catalyze the reaction in three subsequent steps. First, CO reacts with a lattice oxygen at the Au/ZrO_2 interface, forming CO_2 with an energy barrier of 0.79 eV and a reaction energy of −0.83 eV (Figure 6). Then, in a second step an O_2 molecule dissociates at the interface with an energy barrier of 0.33 eV, and the vacancy is refilled with a similar barrier (ΔE^{TS} = 0.43 eV). Finally, in the last step a second CO molecule reacts with the O adatom forming CO_2 with a barrier of 0.81 eV and an energy gain of −0.69 eV. The key aspect is that the formation energy of a surface O vacancy decreases from 5.79 eV without gold to 2.43 eV in the presence of gold.

Before the conclusion of this section, it is useful to mention that the generation of O vacancies at the metal/oxide interface can also lead to other reactions. In a careful theoretical/experimental study on Au/$CeO_{0.62}Zr_{0.38}O_2$ catalyst in CO oxidation, it has been shown that the presence of CO_2 in the gas phase retards the CO oxidation process. This is due to the fact that CO_2 interacts with the O vacancies at the cluster/surface boundary, forming stable carbonates and thus hindering the replenishment of the vacancy by molecular oxygen.[101] This is a nice underreaction demonstration of the metal-assisted MvK mechanism for CO oxidation.

2.4. Water-Gas Shift Reaction. Another process affected by the easier formation of oxygen vacancies near the interface with supported metal particles is the water-gas shift (WGS) reaction:

$$CO + H_2O \rightarrow CO_2 + H_2$$

The reaction has $\Delta H^{\circ}_{298\,K}$ = −41.1 kJ/mol but is kinetically hindered. The general assumption is that there is a direct involvement of the oxide support in the reaction, and in particular two mechanisms have been proposed: (a) a redox mechanism,[102,103] where CO adsorbed on the metal phase is oxidized to CO_2 by labile oxygen of the support and then the support is reoxidized by water, with formation of H_2, and (b) an associative mechanism,[104] which proceeds via the interaction

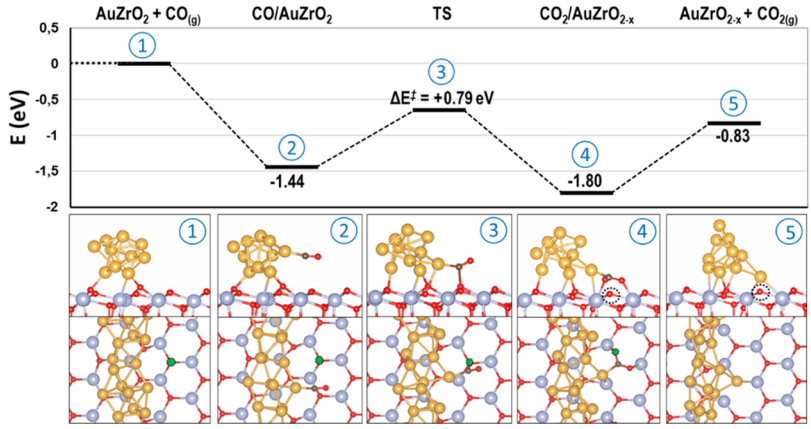

Figure 6. (top) Reaction energy profile and (bottom) side and top views of the structures of the CO oxidation reaction with a surface O_{latt}. The O_{latt} abstracted is indicated by a green filled circle and the O vacancy by a dotted circle. Zr is represented by blue atoms, O by red atoms, Au by golden atoms, and C by brown atoms. Reprinted with permission from ref 100. Copyright 2017 John Wiley and Sons.

DOI: 10.1021/acscatal.7b01913
ACS Catal. 2017, 7, 6493−6513

of adsorbed CO with the hydroxyl groups of the oxide surface leading to a formate intermediate, which then decomposes to CO_2 and H_2.

In a kinetic and mechanistic study of the reaction over a Pt/TiO_2 catalyst, Kalamaras et al. found,[105] on the basis of various transient ^{18}O-isotopic exchange experiments, that the WGS reaction on the Pt/TiO_2 catalyst occurs via a redox mechanism, where CO adsorbs on Pt, diffuses toward the metal−support interface, and then reacts with labile oxygen of the titania support at the metal−support interface to form CO_2 (Figure 7).

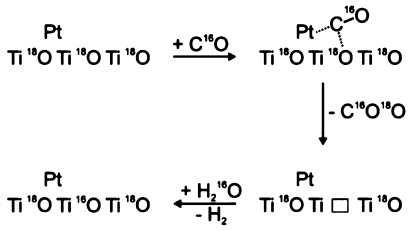

Figure 7. Proposed elementary reaction steps of the WGS reaction over 0.5 wt % Pt/TiO_2 catalyst after $^{16}O/^{18}O$ exchange followed by a $C^{16}O/H_2{}^{16}O$ WGS reaction (T = 200 °C). Reprinted with permission from ref 105. Copyright 2006 Elsevier Ltd.

The reaction has been studied in great detail in an extensive ab initio thermodynamic study by Ammal and Heyden[106,107] and recently extended to Pt/CeO_2 catalysts.[108] It has been observed that the computed energy to remove an oxygen atom from the surface of TiO_2, between 3 and 5 eV depending on the method used, is too high in comparison to the small apparent activation barrier (0.3−0.5 eV) of the catalyzed WGS reaction. However, Pt clusters of various size deposited on the rutile TiO_2(110) surface decrease the V_O formation energy. The effect is larger for the smaller Pt clusters, in agreement with previous literature results from the same group.[82] For the larger Pt clusters (e.g., Pt_8), this converges to a decrease in the V_O formation energy by about 0.7−0.9 eV. On the basis of the DFT results, a thermodynamic analysis has been performed as a function of the oxygen partial pressure and temperature. Entropy effects have also been considered so that the results are based on Gibbs free energies, showing that the presence of Pt clusters promotes the reducibility of the titania surface and the formation of oxygen vacancies at the Pt/TiO_2 interface and that the process becomes thermodynamically favorable under reducing conditions (Figure 8).[106] This is consistent with (a) EPR measurements which indicate that Ti^{3+} ions are formed when Pt/TiO_2 is reduced at 250 °C[109] and (b) temperature-programmed desorption experiments showing that Pt/TiO_2 exposed to CO is reduced at low temperatures.[110]

The critical role of oxygen vacancies at the interface between a Pt_8 cluster and TiO_2 in the WGS reaction has been further demonstrated in a microkinetic model determined from first-principles calculations by the same group.[107] Different routes have been considered for the WGS reaction at Pt/TiO_2 (Figure 9). The computed rates suggest that the CO-promoted redox pathway dominates in the lower temperature range of 473−623 K, while the classical redox pathway becomes dominant for higher temperatures (>623 K). According to this study, the oxygen vacancies formed during the reaction should not be too stable and should also be able to activate H_2O in order to complete the reaction with release of molecular hydrogen.

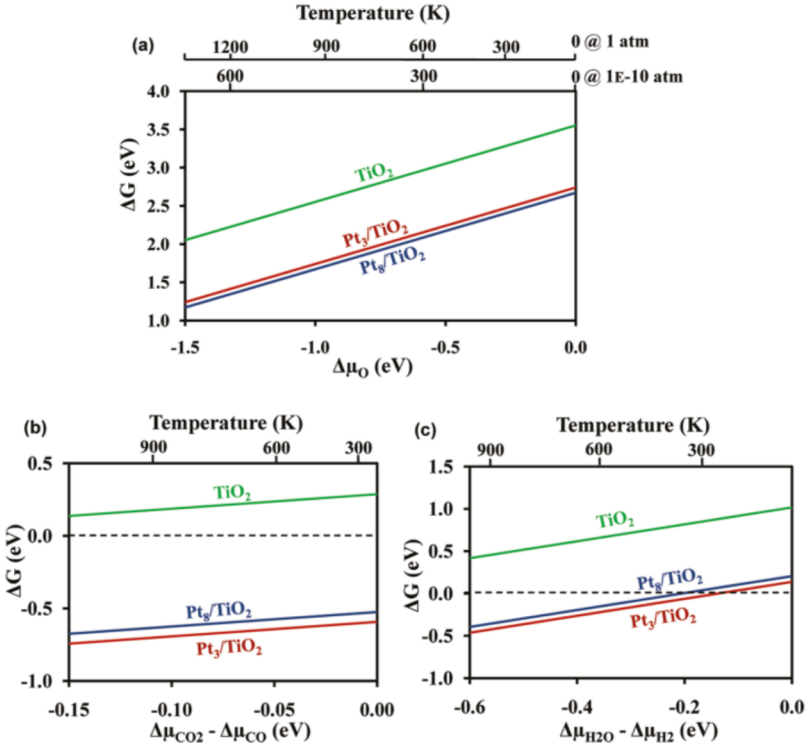

Figure 8. (a) Gibbs free energy (ΔG) for the formation of an oxygen vacancy on the TiO_2 surface ($TiO_2 \rightarrow TiO_{2-x} + 1/2O_2$) versus oxygen chemical potential, $\Delta\mu$(O). (b, c) Gibbs free energy (ΔG) for the formation of an oxygen vacancy on the TiO_2 surface under reducing conditions ($TiO_2 + CO/H_2 \rightarrow TiO_{2-x} + CO_2/H_2O$) versus the difference in chemical potentials $\Delta\mu(CO_2) - \Delta\mu(CO)$ and $\Delta\mu(H_2O) - \Delta\mu(H_2)$, respectively. Reprinted with permission from ref 106. Copyright 2011 American Chemical Society.

DOI: 10.1021/acscatal.7b01913
ACS Catal. 2017, 7, 6493−6513

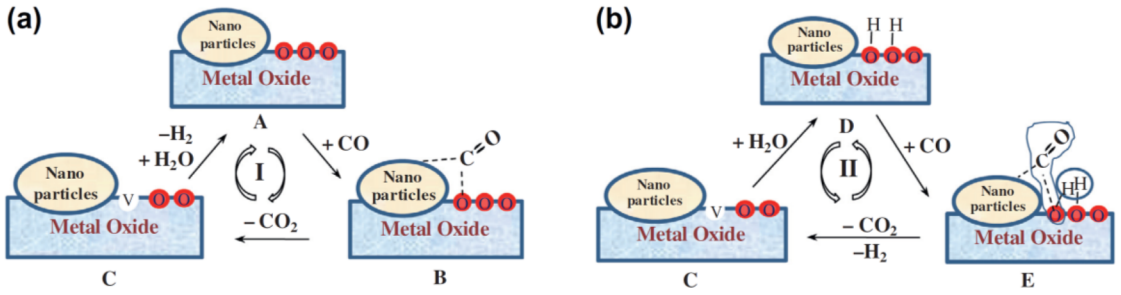

Figure 9. Proposed reaction pathways for the WGS at the TPB that involve surface oxygen atoms: (a) classical redox pathway and (b) associative pathway with redox regeneration. Reprinted with permission from ref 107. Copyright 2013 Elsevier Ltd.

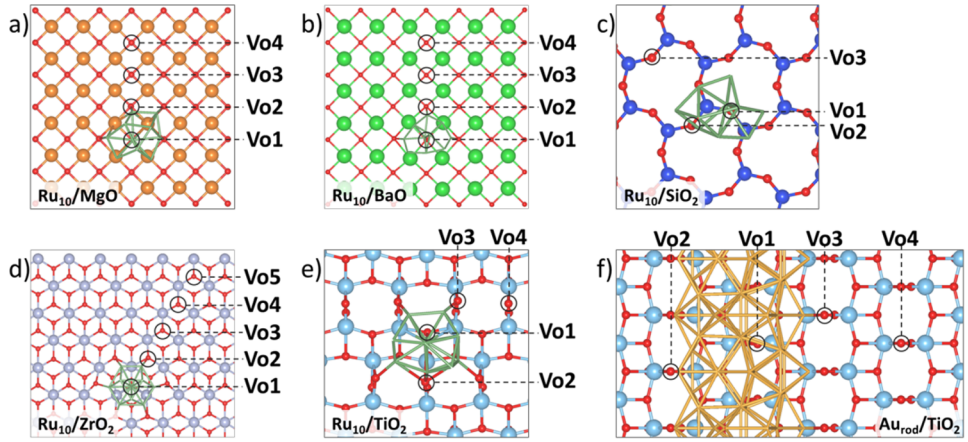

Figure 10. Top views of (a) Ru_{10}/MgO, (b) Ru_{10}/BaO, (c) Ru_{10}/SiO_2, (d) Ru_{10}/ZrO_2, (e) Ru_{10}/TiO_2, and (f) Au_{rod}/TiO_2. The metal−metal bonds of the Ru_{10} cluster are shown in green (a−e), and those of the Au_{rod} are shown in yellow (f). V_On labels refer to the sites where oxygen vacancies are created. The images represent the actual size of the adopted surpercell.

Similar experiments have been performed on ceria-supported metals. Au/CeO_2[111,112] and Cu/CeO_2[111,113] catalysts were reduced under exposure to the WGS ($CO + H_2O$) reaction mixture, while clean CeO_2 remained stoichiometric. The CO molecule is adsorbed on the metal particle and then is desorbed as CO_2 by either detaching a lattice O or by forming carbonate- or formate-like surface species that in turn decompose into CO_2. The O vacancy left on the surface once the CO_2 is formed is stabilized by the metal particle, and it is reoxidized by dissociating the incoming H_2O molecules and releasing H_2, which is the rate-limiting step in the WGS reaction. Thus, the presence of the metal particles is the key to catalyzing the WGS process.

3. VACANCY FORMATION ENERGIES AT METAL/OXIDE INTERFACE

From the above discussion it emerges that the formation energy of an oxygen vacancy is an excellent descriptor of the reactivity of an oxide surface in oxidation reactions. However, the energy costs to create a vacancy can be very different in the bulk or on the surface of an oxide and can change significantly at the metal/oxide interface. This raises some questions. How important is the decrease in the V_O formation energy at the periphery of a supported metal particle? Does this depend on the supported metal? Is it related to the size of the supported nanoparticle? Does it affect only the O atoms at direct contact with the nanoparticle or also the second or more distant neighbors? In order to partially answer these questions, we have performed some novel DFT calculations. The adoption of the same computational setup allows us to compare on an equal footing V_O formation energies as a function of a few parameters: oxide, supported metal, V_O distance from the metal nanoparticle, etc. In this respect, it is not the absolute value of $E_f(V_O)$ that matters but rather its changes. We have considered nonreducible oxides such as MgO, BaO, and SiO_2, a scarcely reducible oxide such as ZrO_2, and a reducible oxide, TiO_2. In all cases, the deposition of a Ru_{10} cluster has been considered. The choice of Ru is due to the fact that this metal has been used to improve the performances of oxide catalysts in biomass conversion,[114,115] a reaction recently studied in detail by our group.[116,117] The effect of the metal and of the particle size has been addressed for the TiO_2 anatase (101) surface comparing a Ru_{10} cluster with a Au periodic nanorod.

The most stable surface of each oxide is adopted, namely (100) in the case of MgO and BaO, while for zirconia and titania we studied the (101) surfaces of the tetragonal and anatase polymorphs, respectively. In the case of silica, we focus on the reconstructed α-quartz (001) surface.[118] In all cases, we recur to the PBE(+U)+D2′ approach to describe the electronic structures, where the two main drawbacks of GGA functionals (the underestimation of the oxide band gap due to the self-interaction error and the underestimation of long-range dispersive forces) are corrected respectively by adding a Hubbard U parameter to the d orbitals of the transition metals[119,120] and ad hoc semiempirical C6 coefficients.[121] A complete description of the computational scheme is reported in the Supporting Information. A top view of the surfaces and considered V_O sites is shown in Figure 10.

For all systems, the effect of the supported metal cluster on the V_O formation energy is studied as a function of the distance

DOI: 10.1021/acscatal.7b01913
ACS Catal. 2017, 7, 6493−6513

between V_O and the metal cluster. For this purpose, a general descriptor R of the vacancy-cluster distance is introduced. When a vacancy is formed on a surface of a generic XO_n system in the presence of a supported M_n' metal particle, R is defined as the minimum distance between any metal atom M of the supported particle and a X cation surrounding the oxygen vacancy (Figure 11).

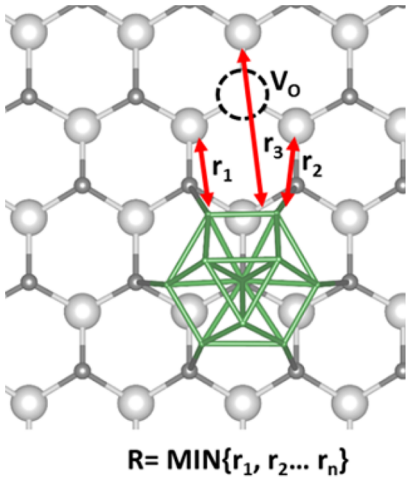

Figure 11. Definition of the vacancy−cluster distance R.

In Table 2, we report the formation energy of a surface V_O defect (E_f, defined with respect to the pristine oxide and 1/2 O_2) on clean surfaces or in the presence of supported metal aggregates. On the clean surfaces, the V_O formation energy varies significantly, spanning from about 6 eV (MgO, ZrO_2) to about 5 eV (BaO, SiO_2). In the case of anatase TiO_2, the (101) surface displays both two-coordinated and three-coordinated O ions; E_f is 4.53 eV in the former case and 5.67 eV in the latter. The nature of the reduced centers also differs from oxide to oxide: while closed-shell F centers are formed on MgO, BaO, and ZrO_2, in the case of TiO_2 the formation of Ti^{3+} is observed. In SiO_2 a covalent Si−Si bond is formed upon oxygen removal.7

In Figure 12, the change in E_f, ΔE_f, due to a supported metal cluster is displayed as a function of the cluster−vacancy distance R (see also Table 2). One can immediately see that, for vacancy−cluster distances as large as 5 Å, ΔE_f tends to 0 in all cases. This means that the effect of the metal particle on the formation of oxygen vacancies is a short-range effect. A certain case dependence, however, emerges when the effect is analyzed at small vacancy−particle distances. The strongest influence is reported in the case of Ru_{10}/SiO_2, where at R = 2.28 Å E_f drops from 4.85 eV (clean oxide) to either 1.87 or 3.11 eV, depending on whether the vacancy site is located underneath the Ru_{10} particle (V_O1) or at its boundaries (V_O2). ΔE_f drops to 0 already at a distance of 4.94 Å (V_O3).

In addition, in the case of Ru_{10}/ZrO_2 the formation energy remarkably decreases at short distances (ΔE_f is −2.51 eV for V_O1 underneath the cluster and −0.94 eV for the boundary case, V_O2). At R = 3.93 Å (V_O3), a moderate ΔE_f value is still found (−0.58 eV), while convergence to the clean-surface E_f value is reached for R > 7 Å (V_O4 and V_O5). On the other oxides, the effect of the Ru_{10} particle on E_f is smaller. For Ru_{10}/TiO_2, for instance, the removal of a three-coordinated oxygen under the cluster (V_O1) costs 3.90 eV (in comparison to 5.67 eV on the clean oxide) with an energy gain of −1.77 eV. In this case, the creation of a vacancy in two nonequivalent peripheral O_{2c} sites (V_O2 and V_O3) leads to rather different results. For V_O2, ΔE_f is −1.75 eV, while for V_O3 it is only −0.22 eV. This strong site dependence can be explained by the remarkable distortion that the Ru_{10} particle undergoes upon adsorption on anatase (101).[122] In the case of V_O2, the closest Ru atom is undercoordinated and is prone to bind strongly to the oxygen vacancy, while in the case of V_O3, the closest Ru atoms exhibit less flexibility. At larger distances, there is even a mild destabilizing effect of the supported nanoparticle (ΔE_f = +0.09 at 4.70 Å).

For more ionic oxides, MgO and BaO, the effect of the Ru_{10} particle on the V_O formation energy is smaller than that in the previous cases and vanishes quite rapidly on moving away from the metal cluster. For Ru_{10}/MgO, ΔE_f = −1.60 eV is reported for the vacancy underneath the cluster (V_O1), which decreases to −1.29 eV if the vacancy is located at a peripheral position (V_O2). At R = 3.04 Å (V_O3), ΔE_f is as small as −0.42 eV, while the formation energy on the clean surface is almost recovered at a distance of 5.53 Å (V_O4). On BaO, the stabilizing effect of Ru_{10} is weak. A gain in energy of −0.44 eV is found for V_O1 (vacancy under the cluster), while in the peripheral site, V_O2, the oxygen vacancy is destabilized by 0.14 eV with respect to the pristine oxide. We attribute this to the strain imposed by the cluster by the surface ions, which hinders the lattice distortion and polaron formation when the vacancy is created. At R > 3 Å (V_O3 and V_O4), ΔE_f is virtually zero (Table 2 and Figure 12).

Interestingly, a very similar trend is reported for Au_{rod} supported on anatase TiO_2 (101). Namely, the stabilizing effect of the rod on the oxygen vacancy is larger when the vacancy lies underneath the Au nanostructure (V_O1, ΔE_f = −1.75 eV). On peripheral sites, there is a residual stabilization of −0.90 eV (V_O2) and −0.45 eV (V_O3). At a distance R = 6 Å, there is no sizable effect of the Au rod. This suggests that the trend is independent of the metal, with small differences between small metal clusters and metal nanostructures due to the different structural flexibility.

The decrease in the formation energy of a V_O center near a metal cluster described above, however, is not universal. In a study of small Pt clusters deposited on the $CeO_2(111)$ surface Bruix et al. found, using a DFT+U approach, that the presence of a Pt_8 cluster has a rather small effect, reducing the cost of V_O formation by 0.2 eV only when the vacancy is directly under the cluster.[123] Along the same line are the results reported by Negreiros and Fabris for the same system using the DFT+U approach.[124] These authors studied the stability of a Pt_4 and a Pt_6 cluster deposited on the same $CeO_2(111)$ surface. They compared the stability of the two Pt clusters on the surface with and without an oxygen vacancy and studied the effect as a function of the position of the vacancy from the cluster. The cluster binding energies to the defective ceria surfaces are reported in Figure 13 and clearly increase as the distance between the cluster and the vacancy increases. Both Pt_4 and Pt_6 clusters show a clear preference to bind on the pristine ceria surface. Formation of O vacancies at the Pt/CeO_2 interface is thus disfavored in comparison to that at the pristine surface, at variance with other oxides. The computed driving force for displacing the vacancy far from the metal/oxide interface is 1.20 eV for Pt_4 and reduces to 0.45 eV for Pt_6.

This behavior has its origin on the fact that Pt clusters deposited on ceria reduce the oxide support by direct electron transfer: i.e., without the need to change the oxide

DOI: 10.1021/acscatal.7b01913
ACS Catal. 2017, 7, 6493−6513

Table 2. Oxygen Vacancy Formation Energies (E_f, eV), Changes in the Formation Energy in the Presence of a Supported Nanoparticle (ΔE_f, eV), Vacancy−Metal Particle Distancse (R, Å) and Bader Charges of the Supported Metal Particles (q_M, |e|)

oxide	system	E_f (eV)	ΔE_f (eV)	R (Å)	q_M (|e|)
MgO	MgO_{1-x}	+6.19			
	Ru_{10}/MgO_{1-x}, V_O1	+4.59	−1.60	2.73	−2.00
	Ru_{10}/MgO_{1-x}, V_O2	+4.90	−1.29	2.67	−2.02
	Ru_{10}/MgO_{1-x}, V_O3	+5.77	−0.42	3.04	−0.82
	Ru_{10}/MgO_{1-x}, V_O4	+6.24	+0.05	5.53	−0.75
	Ru_{10}/MgO				−0.75
BaO	BaO_{1-x}	+4.91			
	Ru_{10}/BaO_{1-x}, V_O1	+4.47	−0.44	3.07	−1.75
	Ru_{10}/BaO_{1-x}, V_O2	+5.05	+0.14	3.24	−1.71
	Ru_{10}/BaO_{1-x}, V_O3	+4.82	−0.09	3.62	−1.21
	Ru_{10}/BaO_{1-x}, V_O4	+4.87	−0.04	7.13	−1.21
	Ru_{10}/BaO				−0.83
ZrO_2	ZrO_{2-x}	+5.92[a]			
	Ru_{10}/ZrO_{2-x}, V_O1	+3.41	−2.51	2.74	−0.52
	Ru_{10}/ZrO_{2-x}, V_O2	+4.98	−0.94	2.66	−0.59
	Ru_{10}/ZrO_{2-x}, V_O3	+5.34	−0.58	3.93	−0.12
	Ru_{10}/ZrO_{2-x}, V_O4	+5.87	−0.05	7.07	−0.07
	Ru_{10}/ZrO_{2-x}, V_O5	+5.87	−0.05	8.97	−0.08
	Ru_{10}/ZrO_2				+0.23
SiO_2	SiO_{2-x}	+4.85			
	Ru_{10}/SiO_{2-x}, V_O1	+1.87	−2.98	2.28	+0.30
	Ru_{10}/SiO_{2-x}, V_O2	+3.11	−1.74	2.28	−0.03
	Ru_{10}/SiO_{2-x}, V_O3	+4.77	−0.08	4.94	+0.11
	Ru_{10}/SiO_2				+0.15
TiO_2	TiO_{2-x} (O_{2c})	+4.53			
	TiO_{2-x} (O_{3c})	+5.67			
	Ru_{10}/TiO_{2-x}, V_O1 (O_{3c})	+3.90	−1.77	2.56	+0.83
	Ru_{10}/TiO_{2-x}, V_O2 (O_{2c})	+2.79	−1.75	2.57	+0.67
	Ru_{10}/TiO_{2-x}, V_O3 (O_{2c})	+4.32	−0.21	2.51	+0.88
	Ru_{10}/TiO_{2-x}, V_O4 (O_{2c})	+4.62	+0.09	4.70	+1.48
	Ru_{10}/TiO_2				+1.53
	Au_{rod}/TiO_{2-x}, V_O1 (O_{2c})	+2.82	−1.75	2.64	−0.76
	Au_{rod}/TiO_{2-x}, V_O2 (O_{2c})	+3.68	−0.90	2.61	−0.24
	Au_{rod}/TiO_{2-x}, V_O3 (O_{2c})	+4.12	−0.45	2.77	−0.34
	Au_{rod}/TiO_{2-x}, V_O4 (O_{2c})	+4.58	0	5.96	−0.09
	Au_{rod}/TiO_2				+0.09

[a]This value has been obtained with a three-layer slab of a 7 × 4 supercell ($Zr_{168}O_{336}$).

stoichiometry. Removing oxygen leads to an additional formation of Ce^{3+} ions, with local distortions and structural relaxation costs. We can conclude that the reduction of the V_O formation energy is expected for oxides which are not already highly reduced or where the deposition of the metal does not lead to an electron-rich surface by the effect of metal to oxide charge transfer.

This introduces another topic, the oxide reduction at the metal/oxide interface due to the charge transfer or charge polarization between the supported metal and the oxide surface. In the cases discussed above, the deposition of Ru_{10} on the stoichiometric oxide surfaces does not cause the effective formation of reduced centers. From the Bader formalism (Table 2), however, the charge transfer at the interface significantly differs from oxide to oxide. On MgO and BaO, the Ru_{10} cluster is reduced (the total Bader charge of the metal particle is −0.75 |e| for MgO and −0.83 |e| for BaO). On ZrO_2 (q_M = +0.23 |e|) and SiO_2 (q_M = +0.15 |e|) the charge transfer at the interface is almost negligible. On TiO_2, the Bader charge of the Ru_{10} cluster is quite large and positive (q_M = +1.53 |e|). However, as previously discussed,[122] it has not been possible to stabilize any Ti^{3+} center in the oxide upon deposition of the Ru_{10} particle, suggesting that the positive charge of the cluster is due to the formation of covalent polar Ru−O bonds, rather than to a net electron transfer to the Ti 3d empty states. More details on the charge transfer at the oxide/cluster interface are discussed in the Supporting Information.

4. OXIDE FILMS AND NANOSTRUCTURES ON METALS: INVERSE CATALYSTS

A particular case of metal/oxide interfaces is represented by ultrathin oxide films and oxide nanostructures grown on a metal

DOI: 10.1021/acscatal.7b01913
ACS Catal. 2017, 7, 6493−6513

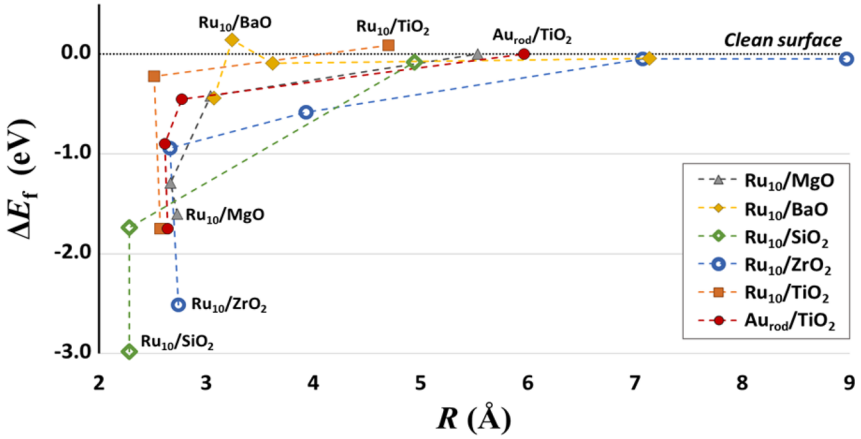

Figure 12. Change in the oxygen vacancy formation energy (ΔE_f, eV) as a function of the vacancy−metal cluster distance (R in Å; see text and Figure 11 for definition).

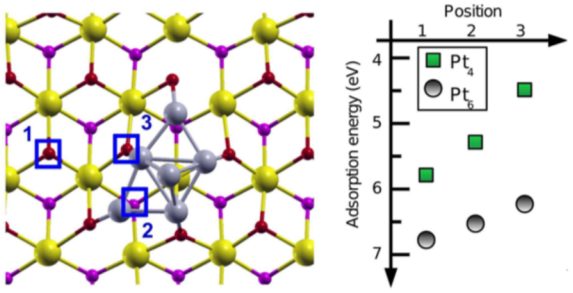

Figure 13. Adsorption energies (in eV, right panel) of Pt_4 and Pt_6 clusters on a defective $CeO_2(111)$ surface with an O vacancy in three different positions (see sites 1−3 in left panel). Reprinted with permission from ref 124. Copyright 2014 American Chemical Society.

support.[125−127] The field of oxide thin films on metals started around 1990, with the aim of obtaining model systems suitable for a better characterization of oxide surfaces. The initial idea was that, by depositing a thin oxide film consisting of a few atomic layers (with thickness typically below 10 nm), one can produce realistic models of oxide surfaces with the advantage of allowing the use of classical characterization tools used in surface science for metals and semiconductors. In particular, depositing ultrathin oxide films on a metal helps overcoming problems connected to the insulating and brittle nature of most oxides. Indeed, great advances have been done in the field by characterizing oxide films with photoemission spectroscopy (XPS, UPS, etc.) and scanning tunneling microscopy (STM).[125,126] Over the past 20 years, the progress in atomistic characterization and understanding of thin oxide films has been spectacular. However, the basic assumption behind this approach, that a thin oxide film will keep the same electronic and geometric structure of the bulk oxide and its surface, is not always fulfilled. While in some particular but restricted cases oxide ultrathin films closely resemble their bulk counterparts, in many other cases they exhibit structures and properties that have little in common with the parent oxide materials. The reader is referred to a few specific reviews[3,125−127] and books for further info on this topic.[128,129]

There are several reasons why thin oxide films differ in general from oxide surfaces. One is that there is a close contact with the metal support, with formation of a metal/oxide interface. This provides an infinite electron reservoir; if the Fermi level of the metal is above the empty states of an adsorbate, and the film is sufficiently thin, electrons can tunnel from the metal to the adsorbate through the insulating layer.[125,126] The opposite is also possible: i.e., species adsorbed on these insulating layers can donate electronic charge to a metal support with high work function. This opens the possibility of tuning the charge state and the surface dipole of a metal/oxide interface. If metal clusters or other adsorbates are deposited on the thin oxide films, additional possibilities arise for the design of nanocatalysts with tailored properties.[126]

It is not surprising that defects such as oxygen vacancies, created in the oxide phase, can also exchange electrons with the metal support, resulting in a charging or discharging of the

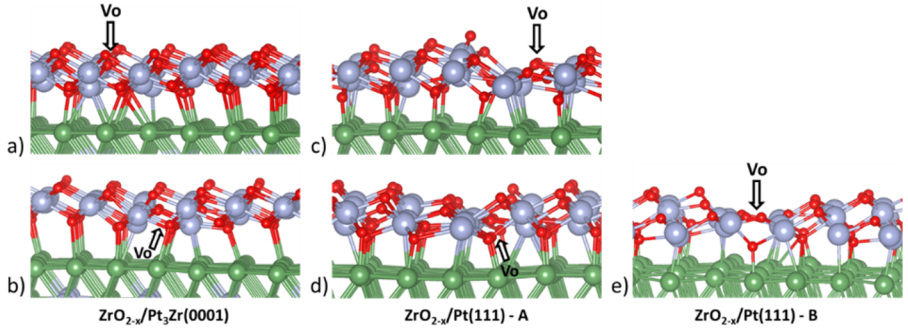

Figure 14. Structures of a ZrO_{2-x} ultrathin film supported on (a, b) $Pt_3Zr(0001)$ (3 × 3) supercell, (c, d) Pt(111) (5 × 5) supercell (A), and (e) Pt(111) ($\sqrt{19}$x$\sqrt{19}$)R23.4° supercell (B). Color scheme: Pt, green; Zr, blue; O, red. The vacancy is indicated with an arrow. Reprinted with permission from ref 133. Copyright 2017 Royal Society of Chemistry.

DOI: 10.1021/acscatal.7b01913
ACS Catal. 2017, 7, 6493−6513

defect states associated with the vacancies, depending on the position of the Fermi level of the metal/oxide interface.[130] This effect has been studied, for instance, for the case of V_O centers created at the top or in interface layers of MgO films grown on Ag(001) or Mo(001).[131] The nature of the oxygen vacancy in these systems, with two, one, or no electrons trapped in the vacancy, depends on several factors, including the metal support, the position of the vacancy in the oxide film, etc. Furthermore, the V_O formation energy in MgO/Ag ultrathin films is lower than that on the regular MgO surface.[132] This shows that nanostructuring a nonreducible oxide such as MgO, and creating a contact with a metal, can result in a change in its intrinsic properties.

Another example is that of zirconia films.[133] As we mentioned before, zirconia is notoriously a hardy reducible oxide. This is consistent with a relatively high formation energy of V_O either in the bulk (6.16 eV) or on the (101) surface of the material (6.03 eV). Things change completely when a two-dimensional (2D) film of zirconia is considered. 2D zirconia does not exist in nature, but ZrO_2/Pt_3Zr and ZrO_2/Pt films (Figure 14) have been prepared and characterized experimentally.[134−140] Using a DFT+U approach with inclusion of dispersion corrections, the process of the chemical reduction of these films by removing oxygen has been studied,[133] showing that the zirconia films exhibit a high reducibility, at variance with the bulk material.

The general underlying principle is that the extra charge introduced when a neutral O vacancy is formed is transferred to the metal substrate. This leads to a dramatic drop in the cost of formation of the vacancy (Table 3). In particular, there is a decrease by a factor of 2 for zirconia films supported on Pt_3Zr and a factor of 6 for Pt supports. Depending also on the position of the vacancy, top or interface layers, $E_f(V_O)$ can drop by 3−5 eV (Table 3), with obvious dramatic consequences on the chemical reactivity of the film that is expected to behave completely differently from the extended zirconia surface.

Table 3. Formation Energies, E_f, of a Neutral O Vacancy in ZrO_2 bulk, ZrO_2(101) Surface, and Pt_3Zr- and Pt-Supported ZrO_{2-x} Thin Films[133]

system		E_f (eV)
ZrO_2 bulk[a]	V_O	+6.16
ZrO_2(101) surface[a]	V_O	+6.03
ZrO_{2-x}/Pt_3Zr(0001)	$V_{O,top}$	+3.28
	$V_{O,interface}$	+2.92
ZrO_{2-x}/Pt(111)	$V_{O,top}$	+0.95
	$V_{O,interface}$	+1.17

[a]These values have been obtained with a (1 × 1 × 1) supercell (bulk) and a five-layer slab of a 3 × 2 supercell ($Zr_{60}O_{120}$) (surface).

The low formation energy of O vacancies (enhanced stability) in the supported thin film in comparison to zirconia bulk and surface is the combination of two contributions: (a) the electron transfer from the vacancy to the metal Fermi level (dominant) and (b) the local structural deformation around the vacancy.[133] The metal substrate acts as an electron scavenger, accepting the extra charge from the O-deficient zirconia. The formation of the ZrO_2/Pt_3Zr or ZrO_2/Pt interfaces thus promotes the formation of O vacancies. The mechanism is similar to what is found when metal clusters are deposited on oxygen vacancies, as also in this case the tendency is to transfer the excess electrons associated with the oxide defect to the metal cluster.

The theoretical results on ZrO_2 films await experimental confirmation. A system which, in contrast, has been extensively studied with both theory and experiment in CO oxidation is FeO films supported on Pt(111). On Pt metal, the strong bonding of CO to the Pt metal catalysts results in poisoning effects. FeO_x/Pt catalysts have been studied because of their potential to annihilate the CO poisoning problem and indeed demonstrated a remarkable activity for the preferential oxidation of CO. Model catalytic studies have shown that FeO islands on Pt(111), exposing coordinatively unsaturated ferrous centers at the interface, are the active structures for CO oxidation at 300 K.[141] Here, the active species are the O atoms derived from the dissociation of O_2 molecules at the periphery of the FeO single-layer islands. Sun et al. studied an extended FeO bilayer film on Pt(111) under high pressures and found the formation of an active FeO_2 phase on Pt(111).[72] This new phase consists of a O−Fe−O trilayer, with an O layer at the interface with Pt, an intermediate Fe layer, and an O layer exposed toward vacuum. This new phase, which only forms under O_2 pressure, enhances CO oxidation on Pt(111) at 450 K. Since interfacial oxygen in the FeO_2 trilayer is bonded with Pt, the electron transfer from Pt caused all of the iron ions in FeO_2 to have a formal Fe^{3+} (ferric) oxidation state, as confirmed by DFT calculations (DFT) and X-ray photoelectron spectroscopy (XPS).[142] Pan et al. later found that reducing the surface coverage of FeO_2 to submonolayer could further boost the activity for CO oxidation at 450 K, and hence they suggested the FeO_2−Pt interface as the active phase for CO oxidation.[143] More recently, the problem has been reconsidered in some detail by Giordano et al.,[144] who analyzed the oxygen trapping and extraction characteristics on a large variety of sites, spanning from oxide terraces to different oxide−metal and oxide−oxide boundaries. The calculated O adsorption/desorption energetics is, to a large extent, specific to the nanoscale nature of the supported oxides and is driven by the electron exchange with the underlying metal substrate. In particular, the oxygen removal is easier at the border sites of the FeO_2 islands, where oxygen vacancy formation is accompanied by a substantial electron transfer toward the Pt substrate.[144] The common denominator of these studies is that, due to the direct contact with the metal support, the FeO layer becomes particularly reactive and, in the presence of an O_2 atmosphere, results in the formation of active oxygen lattice species that play a key role in the CO oxidation, following a classical MvK mechanism.

There is another possible contribution that makes supported oxide films more prone to be reduced. This is the strain that originates in supported oxide due to the lattice mismatch with the metal. The role of strain in reducing the cost of oxygen removal has been discussed in an STM study of cerium oxide films supported on Rh(111).[77] By a combination of STM images with DFT calculations it has been possible to show that under reducing conditions the CeO_x layers develop an ordered array of defects that are identified as oxygen vacancies. The metal/oxide interface creates preferential sites for the reduction of ceria; the local surface strain is invoked as a cause of the enhanced reactivity for vacancy formation.

These studies introduce the more general and broad topic of inverse catalysts.[145,146] This topic has received increasing attention in recent years. There are two configurations to combine oxides and metals: (a) the *conventional* configuration

DOI: 10.1021/acscatal.7b01913
ACS Catal. 2017, 7, 6493−6513

consisting of metal nanoparticles supported on an oxide support, as discussed at the beginning of this Perspective, and (b) the so-called *inverse* configuration in which oxide nanoparticles are supported on a metal. In conventional heterogeneous catalysts the metal is finely dispersed and represents the active phase. A number of factors contribute to the higher activity of the nanoparticles in comparison to the extended surfaces, some already having been mentioned: (1) nanosize effects (higher ratio of corners, vertex, edges, and structural defects) and, for very small clusters, quantum-size effects, (2) "fluxionality" of the metal nanoparticles, i.e. their ability to easily undergo structural deformation, and (3) charge transfer processes due to the interaction with the support. In the inverse configuration, the role of the oxide is more pronounced with respect to that of the metal, since now the oxide is supported as nanoparticles on extended metal surfaces. An additional important factor that contributes to increasing the reactivity is the reducibility of the supported oxide nanoparticle, which generally increases by reducing the size of the nanostructure (see also the discussion above on the role of oxide nanoparticles). Of course, strain in the nanoparticle can also play a role.

The field is very broad, and we restrict our discussion here to one illustrative example, that of CeO_x/Cu(111) (inverse) vs Cu/CeO_2(111) (conventional) catalyst in the WGS reaction.[147] In this work it has been shown that the activity is significantly higher in CeO_x/Cu(111) than in Cu/CeO_2(111). The detailed mechanism of the WGS on these inverse catalysts and the precise role of the metal/oxide interface are still a matter of debate.[148] However, a recent study shows that the excellent performance of a CeO_x/Cu catalyst is related to the beneficial role of a high concentration of oxygen vacancies anchored at interfacial sites of the hybrid catalyst.[149] The vacancies play a mediating role in electron transfer and copper/oxygen species activation. In this respect, it seems that concentrating attention on the role of the oxide phase could be more promising than improving the metallic component of the catalyst. This also confirms that the oxide may play a role even more important than that of the metal in the whole catalytic process.

5. OXYGEN REVERSE SPILLOVER

The formation of oxygen vacancies at the boundary between a supported metal particle and an oxide surface is related to another important phenomenon, oxygen reverse spillover. It consists of the diffusion of oxygen atoms (either those adsorbed or those from the support) to a supported metal nanoparticle that, eventually, can be covered by a more or less thick oxide layer. The phenomenon occurs in a variety of reactions. It was deduced from experimental observations already in the early 1990s.[150,151] Generally, two cases of oxygen spillover can be distinguished. In the first case, oxygen from the gas phase adsorbs on the oxide support and is spilled over to the metal particles. In the second case, oxygen from the oxide lattice is spilled over to the metal, resulting in a reduction of the support and an oxidation of the particle. The latter case can be seen as a first step in what is sometimes referred to as a strong metal−support interaction (SMSI). Under these conditions, an oxide layer grows over the metal particle which, in some cases, can become completely encapsulated, losing its chemical properties and leading to catalyst deactivation. In the context of this Perspective, we focus on the second case and examine just a few illustrative examples.

Precious metals supported on ceria (CeO_2) are widely used catalysts in oxidation reactions, due to the remarkable OSC of ceria, which allows the catalyst to supply lattice oxygen in an excess of reductants and become reoxidized in an excess of oxidants.[39] The underlying mechanism for this transient behavior may be facilitated by the presence of metal particles, involving oxygen reverse spillover from the ceria to the metal. Pt particles supported on ceria have been widely studied, whereby also the role of the CeO_2 morphology was taken into account. Lykhach et al.[152] have shown in STM and XPS experiments that 1.5 nm thick ceria films supported on Cu(111) are easily reduced by the deposition of Pt particles, due to the reverse spillover of lattice oxygen. They suggested that the oxygen reverse spillover is responsible for the self-cleaning behavior of Pt/CeO_2 after the formation of carbon deposits on Pt. In a DFT+U study on Pt_8/CeO_2(111), Bruix et al.[153] found that oxygen reverse spillover to Pt_8 has an energetic cost of only 1.0 eV, substantially lower than the oxygen vacancy formation energy of 2.3 eV. Vayssilov et al.[42] showed in a DFT+U study that the oxygen reverse spillover to Pt_8 becomes even exothermic when the Pt particles are deposited on a ceria nanoparticle. This shows that nanostructured ceria, in the form of thin films and nanoparticles, exhibits an enhanced tendency to give rise to oxygen reverse spillover, a conclusion supported by a combined DFT+U and resonant photoelectron spectroscopy (RPES) study.[41]

Using global optimization algorithms in combination with DFT+U, Negreiros et al.[154] have shown how oxygen reverse spillover affects the morphology of Pt_3−Pt_6 clusters supported on CeO_2(111). Happel et al.[155] adsorbed CO on a Pt/CeO_2(111)/Cu(111) model catalyst and observed a blue shift of the stretching frequency of CO adsorbed on Pt when the catalyst was thermally treated. They assigned this effect to reverse oxygen overspill from ceria to Pt and the consequent oxidation of the metal particle. Similar effects were also observed for subnanometer Pt clusters on ceria nanowires.[156]

In addition to Pt, oxygen reverse spillover was also observed for other ceria-supported metal particles. For instance, Zafiris et al.[151,157] found experimental evidence for this type of mechanism for Rh/CeO_2 using TPD and steady-state reaction measurements. Smirnov et al.[158] demonstrated via XPD and XRD that under mild heating in UHV (100−144 °C), Pd particles supported on a mixed ceria−zirconia support become oxidized, although no O_2 was supplied via the gas phase, indicating oxygen reverse spillover. Matolin et al.[159,160] observed the formation of Ce^{3+} centers upon deposition of Au and Pd particles on 1.5 nm CeO_2 films supported on Cu(111) via XPS, UPS, and RPES. They assigned the reduction to the formation of Au−O−Ce species. On the basis of mechanistic studies on steam re-forming of methanol over Cu/CeO_2/Al_2O_3, Men et al.[161,162] suggested that oxygen reverse spillover from the ceria to the Cu particles is part of the catalytic cycle. Rh, Co, and Rh−Co bimetallic nanoparticles supported on ceria were investigated in an experimental multitechnique study by Varga et al.[163] They observed reverse oxygen spillover for Rh at elevated temperatures. For the Co particles, encapsulation was observed. The bimetallic particles were less prone to oxygen reverse spillover and encapsulation. Ševčíková et al.[164] found in a combined TPR, TPD, and XPS study that the occurrence of the oxygen reverse spillover in Rh/CeO_2 depends on the oxidation state of the ceria substrate, whereby the spillover was inhibited for reduced ceria: i.e., CeO_{2-x}. Oxygen reverse spillover to Rh was also observed

DOI: 10.1021/acscatal.7b01913
ACS Catal. 2017, 7, 6493−6513

when the Rh particles were supported on mixed ceria−zirconia $(Ce_{0.56}Zr_{0.44})O_{2-x}$.[165] The spillover of ceria lattice oxygen has also been observed for Zr particles supported on $CeO_2(111)$/Cu(111): Shanwei et al.[166] demonstrated the reverse spillover of oxygen to the Zr particles via XPS and STM. Similar effects have been observed for Cu particles supported on ceria: Chen et al.,[167] using XPS, IRAS, Raman, and HRTEM, have shown that oxygen vacancies are generated as a consequence of electron donation from metal copper atoms to CeO_2 and subsequent reverse spillover of oxygen.

Oxygen reverse spillover also occurs on oxides other than ceria. In the following, a few examples are summarized. Martin et al.[168] have shown that the exchange rate of ^{18}O isotopes (from gas-phase $^{18}O_2$) with ^{16}O isotopes from the supporting oxide is strongly enhanced in the presence of the Rh nanoparticles supported on SiO_2, Al_2O_3, ZrO_2, MgO, CeO_2, and CeO_2−Al_2O_3, respectively. Using AFM and XPS, Ono et al.[169] found that, upon heating of silica-supported Au clusters to elevated temperatures (T > 1300 K), the silica decomposes at the Au perimeter. The results revealed a Au-assisted oxygen desorption from the support via reverse oxygen spillover to the Au nanoparticles. Chen et al.[170] have shown in a DFT+U study that for Ru_{10} clusters supported on titania anatase and tetragonal zirconia, respectively, the energetic cost for oxygen reverse spillover is relatively low, i.e. 0.2 eV for titania, and has a moderate cost (0.6 eV) for zirconia. Similarly, the energetic cost for oxygen reverse spillover for Ni_{10} supported on the same surfaces was found to be thermoneutral for titania and only slightly endothermic for zirconia (0.6 eV).[171]

These results clearly indicate that the phenomenon of oxygen reverse spillover is very common, when the catalytic process implies high thermal treatments. It is only another manifestation of the same phenomenon, higher oxide reducibility in the proximity of the metal/oxide interface.

6. CONCLUSIONS

In this Perspective, we have analyzed several examples of processes that are directly affected by the formation of a metal/oxide interface. This is common in heterogeneous catalysts based on supported nanoparticles. The atoms of the oxide support in direct contact with the metal particle, and in particular the O atoms at the boundary region, exhibit a different reactivity in comparison to the other O atoms of the surface. In particular, they can be more easily removed by an adsorbed species that is thus oxidized, leaving behind an oxygen vacancy. This important conclusion has been predicted by various theoretical studies and, more recently, verified and supported by specific experiments, as shown in Table 1. The higher reactivity of lattice oxygen at the metal/oxide boundary can be used to design better catalysts in oxidation reactions on going from pure oxide materials to oxide surfaces where metal nanoparticles have been deposited. Of course, the efficiency of such a catalyst will depend also on the resistance toward sintering of the small particles. An aspect that is important and has received relatively little attention so far is how the depletion of oxygen at the metal/oxide boundary affects the subsequent removal of oxygen atoms. Most of the results reported in the literature in fact are dealing with the cost of removing the first O atom from the interface, while this cost can be significantly different once the surface starts to be reduced.[172]

The main reason for the easier removal of the oxygen atoms at the cluster boundary is that the metal atoms from the supported cluster can refill the vacancy and partially compensate the relatively high cost to create an anion vacancy in an oxide. In this respect, the structural flexibility of the supported nanoparticle plays an essential role. In addition, the contribution of the metal counterpart in delocalizing the excess electrons arising from the creation of a neutral vacancy is very important. This effect has crucial consequences in all oxidation reactions, but here two cases have been considered in detail: CO oxidation and the water-gas shift reaction.

The study of these two processes has provided compelling evidence of the direct involvement of oxygen atoms at the interface region and of a MvK mechanism. The interesting aspect is that the presence of a supported metal can deeply change locally the chemical behavior of an oxide, to the point that even nonreducible oxides can become partly reducible thanks to this cooperative effect. Since the reducibility of an oxide can also be varied by nanostructuring (nanoparticles, nanowires, ultrathin films, etc.), the potential of metal/oxide interfaces on the nanoscale opens up interesting and largely unexplored possibilities for heterogeneous catalysis.

The phenomenon of higher reducibility at the metal/oxide interface, however, is of general interest and broader impact. Remaining in the field of catalysis, the interplay between metals and oxides plays a key role in the growing field of inverse catalysts or in the more traditional processes of oxygen reverse spillover. Outside catalysis, generation of vacancies at the metal/oxide interface is relevant in the area of memristors.[173] Memristors are systems with several potential applications in microelectronics and can be used for information storage or as logic gates. The interfaces between the metal electrodes and the oxide play a crucial role, especially for bipolar switches. A typical memristor consists of a thin (50 nm) TiO_2 film between two 5 nm thick electrodes (e.g. Ti, Pt, etc.). The deposition of the metal layer on the oxide can result in the formation of oxygen vacancies. These defects are at the basis of the working principle of this kind of memristor. Under an applied electric field, in fact, oxygen vacancies can drift into the interface region, reducing the electronic barrier and resulting in a low-resistance state. Under an electric field with the opposite polarity, the oxygen vacancies are repelled away from the interface region, recovering the electronic barrier to regain the high resistance state. The process is fully reversible, and the device can be used to store or elaborate information. Staying in the field of inorganic semiconductor applications, such as metal oxide semiconductor field-effect transistors (MOS-FETs), chemical reactions and defects at a metal/oxide interface can cause an oxide gate dielectric to have high leakage current, with deterioration of the properties. These simple examples demonstrate that a better understanding of the nature of the metal/oxide interface is essential in a variety of technological areas, not only in catalysis.

■ ASSOCIATED CONTENT

Supporting Information

The Supporting Information is available free of charge on the ACS Publications website at DOI: 10.1021/acscatal.7b01913.

Computational details (methods used, supercell sizes, etc.) for the original calculations described in section 3 together with an analysis of the charge distribution at the metal/oxide interfaces (PDF)

DOI: 10.1021/acscatal.7b01913
ACS Catal. 2017, 7, 6493−6513

AUTHOR INFORMATION

Corresponding Author

*E-mail for G.P.: gianfranco.pacchioni@unimib.it.

ORCID

Philomena Schlexer: 0000-0002-3135-9089
Sergio Tosoni: 0000-0001-5700-4086
Gianfranco Pacchioni: 0000-0002-4749-0751

Notes

The authors declare no competing financial interest.

ACKNOWLEDGMENTS

This work has been supported by the European Community's Seventh Program FP7/2007-2013 under Grant Agreement No.607417—European Marie Curie Network CATSENSE, Grant Agreement No. 604307 (CASCATBEL) and by the Italian MIUR through the PRIN Project 2015K7FZLH SMARTNESS "Solar driven chemistry: new materials for photo- and electro-catalysis". The unpublished calculations included in this paper were realized on the CINECA supercomputing facilities (Grants HP10BD69EF and HPL13PKBV5).

REFERENCES

(1) Campbell, C. T.; Sauer, J. *Chem. Rev.* **2013**, *113*, 3859.
(2) Ferrari, A. M.; Pacchioni, G. *J. Phys. Chem.* **1995**, *99*, 17010—17018.
(3) Pacchioni, G.; Freund, H. J. *Chem. Rev.* **2013**, *113*, 4035—4072.
(4) Jupille, J.; Thornton, G. In *Defects at Oxide Surfaces*; Springer: Heidelberg, Germany, 2015.
(5) Mars, P.; van Krevelen, P. *Chem. Eng. Sci.* **1954**, *3*, 41—59.
(6) Tsuji, H.; Hattori, H. *ChemPhysChem* **2004**, *5*, 733—736.
(7) Pacchioni, G. *ChemPhysChem* **2003**, *4*, 1041—1047.
(8) Nilius, N. *Surf. Sci. Rep.* **2009**, *64*, 595—659.
(9) Lauritsen, J. V.; Foster, A. S.; Olesen, G. H.; Christensen, M. C.; Kühnle, A.; Helveg, S.; Rostrup-Nielsen, J. R.; Clausen, B. S.; Reichling, M.; Besenbacher, F. *Nanotechnology* **2006**, *17*, 3436—3441.
(10) Sterrer, M.; Heyde, M.; Novicki, M.; Nilius, N.; Risse, T.; Rust, H.-P.; Pacchioni, G.; Freund, H.-J. *J. Phys. Chem. B* **2006**, *110*, 46—49.
(11) König, T.; Simon, G. H.; Martinez, U.; Giordano, L.; Pacchioni, G.; Heyde, M.; Freund, H.-J. *ACS Nano* **2010**, *4*, 2510—2514.
(12) Chrétien, S.; Metiu, H. *Catal. Lett.* **2006**, *107*, 143—147.
(13) Shapovalov, V.; Metiu, H. *J. Catal.* **2007**, *245*, 205—214.
(14) Pala, R. G. S.; Metiu, H. *J. Phys. Chem. C* **2007**, *111*, 8617—8622 and references therein.
(15) Thompson, J. L.; Yates, J. T. *Chem. Rev.* **2006**, *106*, 4428—4453.
(16) McFarland, E. W.; Metiu, H. *Chem. Rev.* **2013**, *113*, 4391—4427.
(17) Sato, S. *Chem. Phys. Lett.* **1986**, *123*, 126—128.
(18) Asahi, R.; Morikawa, T.; Ohwaki, T.; Aoki, K.; Taga, Y. *Science* **2001**, *293*, 269—271.
(19) Di Valentin, C.; Pacchioni, G.; Selloni, A. *Phys. Rev. B: Condens. Matter Mater. Phys.* **2004**, *70*, 085116—085119.
(20) Livraghi, S.; Paganini, M. C.; Giamello, E.; Selloni, A.; Di Valentin, C.; Pacchioni, G. *J. Am. Chem. Soc.* **2006**, *128*, 15666—15671.
(21) Finazzi, E.; Di Valentin, C.; Selloni, A.; Pacchioni, G. *J. Phys. Chem. C* **2007**, *111*, 9275—8282.
(22) Albanese, E.; Leccese, M.; Di Valentin, C.; Pacchioni, G. *Sci. Rep.* **2016**, *6*, 31435.
(23) Pesci, M.; Gallino, F.; Di Valentin, C.; Pacchioni, G. *J. Phys. Chem. C* **2010**, *114*, 1350—1356.
(24) Pacchioni, G.; Pescarmona, P. *Surf. Sci.* **1998**, *412-413*, 657—671.
(25) Wichtendahl, R.; Rodriguez-Rodrigo, M.; Härtel, U.; Kuhlenbeck, H.; Freund, H.-J. *Surf. Sci.* **1999**, *423*, 90—98.
(26) Wichtendahl, R.; Rodriguez-Rodrigo, M.; Härtel, U.; Kuhlenbeck, H.; Freund, H.-J. *Phys. Stat. Sol. A* **1999**, *173*, 93—100.
(27) Giamello, E.; Murphy, D.; Marchese, L.; Martra, G.; Zecchina, A. *J. Chem. Soc., Faraday Trans.* **1993**, *89*, 3715—3722.
(28) Spoto, G.; Gribov, E. N.; Ricchiardi, G.; Damin, A.; Scarano, D.; Bordiga, S.; Lamberti, C.; Zecchina, A. *Prog. Surf. Sci.* **2004**, *76*, 71—146.
(29) Di Valentin, C.; Finazzi, E.; Pacchioni, G. *Surf. Sci.* **2005**, *591*, 70—89.
(30) Pacchioni, G.; Ricart, J. M.; Illas, F. *J. Am. Chem. Soc.* **1994**, *116*, 10152—10158.
(31) French, R. H.; Glass, S. J.; Ohuchi, F. S.; Xu, Y. N.; Ching, E. Y. *Phys. Rev. B: Condens. Matter Mater. Phys.* **1994**, *49*, 5133—5142.
(32) Sayan, S.; Bartynski, R. A.; Zhao, X.; Gusev, E. P.; Vanderbilt, C.; Croft, M.; Banaszak-Holl, M.; Garfunkel, E. *Phys. Status Solidi B* **2004**, *241*, 2246—2252.
(33) Gionco, C.; Paganini, M. C.; Giamello, E.; Burgess, R.; Di Valentin, C.; Pacchioni, G. *Chem. Mater.* **2013**, *25*, 2243—2253.
(34) Ruiz Puigdollers, A.; Illas, F.; Pacchioni, G. *J. Phys. Chem. C* **2016**, *120*, 4392—4402.
(35) Ruiz Puigdollers, A.; Illas, F.; Pacchioni, G. *Rend. Fis. Acc. Lincei* **2017**, *28*, 19—27.
(36) Pham, T. N.; Sooknoi, T.; Crossley, S. P.; Resaco, D. E. *ACS Catal.* **2013**, *3*, 2456—2473.
(37) Pacchioni, G. *ACS Catal.* **2014**, *4*, 2874—2888.
(38) Sinhamahapatra, A.; Leon, J. P.; Kang, J.; Han, B.; Yu, J. S. *Sci. Rep.* **2016**, *6*, 27218—27225.
(39) Trovarelli, A. *Catal. Rev.: Sci. Eng.* **1996**, *38*, 439—520.
(40) Loschen, C.; Migani, A.; Bromley, S. T.; Illas, F.; Neyman, K. M. *Phys. Chem. Chem. Phys.* **2008**, *10*, 5730—5738.
(41) Vayssilov, G. N.; Lykhach, Y.; Migani, A.; Staudt, T.; Petrova, G. P.; Tsud, N.; Skála, T.; Bruix, A.; Illas, F.; Prince, K. C.; et al. *Nat. Mater.* **2011**, *10*, 310—315.
(42) Vayssilov, G. N.; Migani, A.; Neyman, K. M. *J. Phys. Chem. C* **2011**, *115*, 16081—16086.
(43) Migani, A.; Vayssilov, G. N.; Bromley, S. T.; Illas, F.; Neyman, K. M. *Chem. Commun.* **2010**, *46*, 5936—5938.
(44) Campbell, C. T.; Parker, S. C.; Starr, D. E. *Science* **2002**, *298*, 811—814.
(45) Loschen, C.; Bromley, S. T.; Neyman, K. M.; Illas, F. *J. Phys. Chem. C* **2007**, *111*, 10142—10145.
(46) Migani, A.; Neyman, K. M.; Illas, F.; Bromley, S. T. *J. Chem. Phys.* **2009**, *131*, 064701—064707.
(47) Pacchioni, G. In *Oxide materials at the two-dimensional limit*; Netzer, F., Fortunelli, A., Eds.; Springer: Heidelberg, Germany, 2016; pp 91—118.
(48) Pacchioni, G. *Catal. Lett.* **2015**, *145*, 80—94.
(49) Pacchioni, G. *Phys. Chem. Chem. Phys.* **2013**, *15*, 1737—1757.
(50) Sanchez, A.; Abbet, S.; Heiz, H.; Schneider, W. D.; Häkkinen, H.; Barbett, R. N.; Landman, U. *J. Phys. Chem. A* **1999**, *103*, 9573—9578.
(51) Yoon, B.; Häkkinen, H.; Landman, U.; Wörz, A. S.; Antonietti, J. M.; Abbet, S.; Judai, K.; Heiz, U. *Science* **2005**, *307*, 403—407.
(52) Remediakis, I. N.; Lopez, N.; Norskov, J. K. *Angew. Chem., Int. Ed.* **2005**, *44*, 1824—1826.
(53) Wörz, A. S.; Heiz, U.; Cinquini, F.; Pacchioni, G. *J. Phys. Chem. B* **2005**, *109*, 18418—18426.
(54) Chrétien, S.; Metiu, H. *J. Chem. Phys.* **2007**, *126*, 104701—104707.
(55) Antonietti, J.-M.; Michalski, M.; Heiz, U.; Jones, H.; Lim, K. H.; Rösch, N.; Del Vitto, A.; Pacchioni, G. *Phys. Rev. Lett.* **2005**, *94*, 213402—213405.
(56) Abbet, S.; Sanchez, A.; Heiz, U.; Schneider, W. D.; Ferrari, A. M.; Pacchioni, G.; Rösch, N. *J. Am. Chem. Soc.* **2000**, *122*, 3453—3457.
(57) Heiz, U.; Schneider, W.-D. *J. Phys. D: Appl. Phys.* **2000**, *33*, R85—R102.
(58) Abbet, S.; Sánchez, A.; Heiz, U.; Schneider, W.-D. *J. Catal.* **2001**, *198*, 122—127.
(59) Sterrer, M.; Yulikov, M.; Fishbach, E.; Heyde, M.; Rust, H.-P.; Pacchioni, G.; Risse, T.; Freund, H.-J. *Angew. Chem., Int. Ed.* **2006**, *45*, 2630—2632.

DOI: 10.1021/acscatal.7b01913
ACS Catal. 2017, 7, 6493—6513

(60) Widmann, D.; Behm, R. J. *Chin. J. Catal.* **2016**, *37*, 1684−1693.
(61) Widmann, D.; Krautsieder, A.; Walter, P.; Brückner, A.; Behm, R. J. *ACS Catal.* **2016**, *6*, 5005−5011.
(62) Li, W.; Ge, Q.; Ma, X.; Chen, Y.; Zhu, M.; Xu, H.; Jin, R. *Nanoscale* **2016**, *8*, 2378−2385.
(63) Lohrenscheit, M.; Hess, C. *ChemCatChem* **2016**, *8*, 523−526.
(64) Altass, H. M.; Khder, A. E. R. S. *Mater. Res. Innovations* **2017**, 1−8.
(65) Bliem, R.; van der Hoeven, J.; Zavodny, A.; Gamba, O.; Pavelec, J.; de Jongh, P. E.; Schmid, M.; Diebold, U.; Parkinson, G. S. *Angew. Chem., Int. Ed.* **2015**, *54*, 13999−14002.
(66) Zhao, K.; Tang, H.; Qiao, B.; Li, L.; Wang, J. *ACS Catal.* **2015**, *5*, 3528−3539.
(67) Widmann, D.; Hocking, E.; Behm, R. J. *J. Catal.* **2014**, *317*, 272−276.
(68) Li, L.; Wang, A.; Qiao, B.; Lin, J.; Huang, Y.; Wang, X.; Zhang, T. *J. Catal.* **2013**, *299*, 90−100.
(69) Maeda, Y.; Iizuka, Y.; Kohyama, M. *J. Am. Chem. Soc.* **2013**, *135*, 906−909.
(70) Widmann, D.; Behm, R. J. *Angew. Chem., Int. Ed.* **2011**, *50*, 10241−10245.
(71) Widmann, D.; Liu, Y.; Schüth, F.; Behm, R. J. *J. Catal.* **2010**, *276*, 292−305.
(72) Sun, Y. N.; Giordano, L.; Goniakowski, J.; Lewandowski, M.; Qin, Z. H.; Noguera, C.; Shaikhutdinov, S.; Pacchioni, G.; Freund, H. J. *Angew. Chem., Int. Ed.* **2010**, *49*, 4418−4421.
(73) Kotobuki, M.; Leppelt, R.; Hansgen, D. A.; Widmann, D.; Behm, R. J. *J. Catal.* **2009**, *264*, 67−76.
(74) Kalamaras, C. M.; Panagiotopoulou, P.; Kondarides, D. I.; Efstathiou, A. M. *J. Catal.* **2009**, *264*, 117−129.
(75) Widmann, D.; Leppelt, R.; Behm, R. J. *J. Catal.* **2007**, *251*, 437−442.
(76) Carrettin, S.; Concepción, P.; Corma, A.; López Nieto, J. M.; Puntes, V. F. *Angew. Chem., Int. Ed.* **2004**, *43*, 2538−2540.
(77) Castellarin-Cudia, C.; Surnev, S.; Schneider, G.; Podlucky, R.; Ramsey, M. G.; Netzer, F. P. *Surf. Sci.* **2004**, *554*, L120−L126.
(78) Green, R.; Morrall, P.; Bowker, M. *Catal. Lett.* **2004**, *98*, 129−133.
(79) Giordano, L.; Goniakowski, J.; Pacchioni, G. *Phys. Rev. B: Condens. Matter Mater. Phys.* **2001**, *64*, 075417−075425.
(80) Giordano, L.; Goniakowski, J.; Pacchioni, G. *Phys. Rev. B: Condens. Matter Mater. Phys.* **2003**, *67*, 045410−045417.
(81) Honkala, K.; Hakkinen, H. *J. Phys. Chem. C* **2007**, *111*, 4319−4327.
(82) Ammal, S. C.; Heyden, A. *J. Chem. Phys.* **2010**, *133*, 164703−164717.
(83) Okumura, M.; Coronado, J. M.; Soria, J.; Haruta, M.; Conesa, J. *J. Catal.* **2001**, *203*, 168−174.
(84) Liu, Z. P.; Gong, X. Q.; Kohanoff, J.; Sanchez, C.; Hu, P. *Phys. Rev. Lett.* **2003**, *91*, 266102−266105.
(85) Remediakis, I. N.; Lopez, N.; Nørskov, J. K. *Angew. Chem.* **2005**, *117*, 1858−1860.
(86) Molina, L. M.; Hammer, B. *Appl. Catal., A* **2005**, *291*, 21−31.
(87) Green, I. X.; Tang, W.; Neurock, M.; Yates, J. T., Jr *Acc. Chem. Res.* **2014**, *47*, 805−815.
(88) Gong, J.; Mullins, C. B. *Acc. Chem. Res.* **2009**, *42*, 1063−1073.
(89) Widmann, D.; Liu, Y.; Schüth, F.; Behm, R. J. *J. Catal.* **2010**, *276*, 292−305.
(90) Widmann, D.; Behm, R. J. *Acc. Chem. Res.* **2014**, *47*, 740−749.
(91) Li, L.; Zeng, X. C. *J. Am. Chem. Soc.* **2014**, *136*, 15857−15860.
(92) Li, L.; Gao, Y.; Li, H.; Zhao, Y.; Pei, Y.; Chen, Z. F.; Zeng, X. C. *J. Am. Chem. Soc.* **2013**, *135*, 19336−19346.
(93) Duan, Z.; Henkelman, G. *ACS Catal.* **2015**, *5*, 1589−1595.
(94) Saqlain, M. A.; Hussain, A.; Siddiq, M.; Ferreira, A. R.; Leitão, A. A. *Phys. Chem. Chem. Phys.* **2015**, *17*, 25403−25410.
(95) Saqlain, M. A.; Hussain, A.; Siddiq, M.; Leitão, A. A. *Appl. Catal., A* **2016**, *519*, 27−33.
(96) Wang, Y. G.; Cantu, D. C.; Lee, M. S.; Li, J.; Glezakou, V. A.; Rousseau, R. *J. Am. Chem. Soc.* **2016**, *138*, 10467−10476.
(97) Kim, H. Y.; Henkelman, G. J. *J. Phys. Chem. Lett.* **2013**, *4*, 216−221.
(98) Li, W.; Ge, Q.; Ma, X.; Chen, Y.; Zhu, M.; Xu, H.; Jin, R. *Nanoscale* **2016**, *8*, 2378−2385.
(99) Hoh, S. W.; Thomas, L.; Jones, G.; Willok, D. J. *Res. Chem. Intermed.* **2015**, *41*, 9587−9601.
(100) Ruiz-Puigdollers, A.; Pacchioni, G. *ChemCatChem* **2017**, *9*, 1119−1127.
(101) del Río, E.; Collins, S. E.; Aguirre, A.; Chen, X.; Delgado, J. J.; Calvino, J. J.; Bernal, S. *J. Catal.* **2014**, *316*, 210−218.
(102) Barbier, J.; Duprez, D. *Appl. Catal., B* **1993**, *3*, 61−83.
(103) Wang, X.; Gorte, R. J.; Wagner, J. P. *J. Catal.* **2002**, *212*, 225−230.
(104) Shido, T.; Iwasawa, Y. *J. Catal.* **1993**, *141*, 71−81.
(105) Kalamaras, C. M.; Panagiotopoulou, P.; Kondarides, D. I.; Efsathiou, A. M. *J. Catal.* **2009**, *264*, 117−129.
(106) Ammal, S. C.; Heyden, A. *J. Phys. Chem. C* **2011**, *115*, 19246−19259.
(107) Ammal, S. C.; Heyden, A. *J. Catal.* **2013**, *306*, 78−90.
(108) Aranifard, S.; Ammal, S. C.; Heyden, A. *J. Catal.* **2014**, *309*, 314−324.
(109) Conesa, J. C.; Soria, J. *J. Phys. Chem.* **1982**, *86*, 1392−1395.
(110) Panagiotopoulou, P.; Christodoulakis, A.; Kondarides, D. I.; Boghosian, S. *J. Catal.* **2006**, *240*, 114−125.
(111) Rodríguez, J. A.; Liu, P.; Hrbek, J.; Evans, J.; Pérez, M. *Angew. Chem.* **2007**, *119*, 1351−1354.
(112) Rodríguez, J. A.; Wang, X.; Liu, P.; Wen, W.; Hanson, J. C.; Hrbek, J.; Pérez, M.; Evans, J. *Top. Catal.* **2007**, *44*, 73−81.
(113) Wang, X.; Rodríguez, J. A.; Hanson, J. C.; Gamarra, D.; Martínez-Arias, A.; Fernández-García, M. *J. Phys. Chem. B* **2006**, *110*, 428−434.
(114) Pham, T. N.; Shi, D. C.; Resasco, D. E. *Top. Catal.* **2014**, *57*, 706−714.
(115) Pham, T. N.; Shi, D. C.; Resasco, D. E. *J. Catal.* **2014**, *314*, 149−158.
(116) Chen, H.-Y.; Pacchioni, G. *ChemCatChem* **2016**, *8*, 2492−2499.
(117) Tosoni, S.; Pacchioni, G. *J. Catal.* **2016**, *344*, 465−473.
(118) Goumans, T. P. M.; Wander, A.; Brown, W. A.; Catlow, C. R. A. *Phys. Chem. Chem. Phys.* **2007**, *9*, 2146−2152.
(119) Anisimov, V. I.; Zaanen, J.; Andersen, O. K. *Phys. Rev. B: Condens. Matter Mater. Phys.* **1991**, *44*, 943−954.
(120) Dudarev, S. L.; Botton, G. A.; Savrasov, S. Y.; Humphreys, C. J.; Sutton, A. P. *Phys. Rev. B: Condens. Matter Mater. Phys.* **1998**, *57*, 1505−1509.
(121) Grimme, S. *J. Comput. Chem.* **2006**, *27*, 1787−1799.
(122) Chen, H. Y. T.; Tosoni, S.; Pacchioni, G. *J. Phys. Chem. C* **2015**, *119*, 10856−10868.
(123) Bruix, A.; Migani, A.; Vayssilov, G. N.; Neyman, K. M.; Libuda, J.; Illas, F. *Phys. Chem. Chem. Phys.* **2011**, *13*, 11384−11392.
(124) Negreiros, F. R.; Fabris, S. *J. Phys. Chem. C* **2014**, *118*, 21014−21020.
(125) Freund, H. J.; Pacchioni, G. *Chem. Soc. Rev.* **2008**, *37*, 2224−2242.
(126) Giordano, L.; Pacchioni, G. *Acc. Chem. Res.* **2011**, *44*, 1244−1252.
(127) Pacchioni, G. *Chem. - Eur. J.* **2012**, *18*, 10144−10158.
(128) In *Oxide Ultrathin Films: Science and Technology*; Pacchioni, G., Valeri, S., Eds.; Wiley-VCH: Weinheim, Germany, 2012.
(129) In *Oxide materials at the two-dimensional limit*; Netzer, F., Fortunelli, A., Eds.; Springer: Heidelberg, Germany, 2016; Vol. *234*.
(130) Shao, X.; Prada, S.; Giordano, L.; Pacchioni, G.; Nilius, N.; Freund, H.-J. *Angew. Chem., Int. Ed.* **2011**, *50*, 11525−11527.
(131) Giordano, L.; Martinez Pozzoni, U.; Pacchioni, G.; Watkins, M.; Shluger, A. *J. Phys. Chem. C* **2008**, *112*, 3857−3865.
(132) Jung, J.; Shin, H.-J.; Kim, Y.; Kawai, M. *J. Am. Chem. Soc.* **2011**, *133*, 6142−6145.
(133) Ruiz Puigdollers, A.; Pacchioni, G. *Nanoscale* **2017**, *9*, 6866−6876.

DOI: 10.1021/acscatal.7b01913
ACS Catal. 2017, 7, 6493−6513

(134) Antlanger, M.; Mayr-Schmölzer, W.; Pavelec, J.; Mittendorfer, F.; Redinger, J.; Varga, P.; Diebold, U.; Schmid, M. *Phys. Rev. B: Condens. Matter Mater. Phys.* **2012**, *86*, 035451−035459.
(135) Li, H.; Choi, J. I. J.; Mayr-Schmölzer, W.; Weilach, C.; Rameshan, C.; Mittendorfer, F.; Redinger, J.; Schmidt, M.; Rupprechter, G. *J. Phys. Chem. C* **2015**, *119*, 2462−2470.
(136) Napetschnig, E.; Schmid, M.; Varga, P. *Surf. Sci.* **2008**, *602*, 1750−1756.
(137) Maurice, V.; Salmeron, M.; Somorjai, G. A. *Surf. Sci.* **1990**, *237*, 116−126.
(138) Meinel, K.; Eichler, A.; Förster, S.; Schindler, K. M.; Neddermeyer, H.; Widdra, W. *Phys. Rev. B: Condens. Matter Mater. Phys.* **2006**, *74*, 235444−235454.
(139) Meinel, K.; Eichler, A.; Schindler, K. M.; Neddermeyer, H. *Surf. Sci.* **2004**, *562*, 204−2018.
(140) Meinel, K.; Schindler, K. M.; Neddermeyer, H. *Surf. Sci.* **2003**, *532-535*, 420−424.
(141) Fu, Q.; Li, W.-X.; Yao, Y.; Liu, H.; Su, H. J.; Ma, D.; Gu, X. G.; Chen, L.; Wang, Z.; Zhang, H.; Wang, B.; Bao, X. *Science* **2010**, *328*, 1141−1144.
(142) Giordano, L.; Lewandowski, M.; Groot, I. M. N.; Sun, Y. N.; Goniakowski, J.; Noguera, C.; Shaikhutdinov, S.; Pacchioni, G.; Freund, H. J. *J. Phys. Chem. C* **2010**, *114*, 21504−21509.
(143) Pan, Q. S.; Weng, X. F.; Chen, M. S.; Giordano, L.; Pacchioni, G.; Noguera, C.; Goniakowski, J.; Shaikhutdinov, S.; Freund, H. J. *ChemCatChem* **2015**, *7*, 2620−2627.
(144) Giordano, L.; Pacchioni, G.; Noguera, C.; Goniakowski, J. *ChemCatChem* **2014**, *6*, 185−190.
(145) Schoiswohl, J.; Surnev, S.; Netzer, F. P. *Top. Catal.* **2005**, *36*, 91−105.
(146) Rodriguez, J. A.; Hrbek, J. *Surf. Sci.* **2010**, *604*, 241−244.
(147) Rodriguez, J. A.; Graciani, J.; Evans, J.; Park, J. B.; Yang, F.; Stacchiola, D.; Senanayake, S. D.; Ma, S.; Pérez, M.; Liu, P.; Sanz, J. F.; Hrbek, J. *Angew. Chem., Int. Ed.* **2009**, *48*, 8047−8050.
(148) Graciani, J.; Sanz, J. F. *Catal. Today* **2015**, *240*, 214−219.
(149) Chen, S.; Li, L.; Hu, W.; Huang, X.; Li, Q.; Xu, Y.; Zuo, Y.; Li, G. *ACS Appl. Mater. Interfaces* **2015**, *7*, 22999−23007.
(150) Li, C.; Chen, Y.; Li, W.; Xin, Q.; Inui, T.; Fujimoto, K.; Uchijima, T.; Masai, M. *Stud. Surf. Sci. Catal.* **1993**, *77*, 217.
(151) Zafiris, G. S.; Gorte, R. J. *J. Catal.* **1993**, *139*, 561−567.
(152) Lykhach, Y.; Staudt, T.; Lorenz, M. P. A.; Streber, R.; Bayer, A.; Steinrück, H. P.; Libuda, J. *ChemPhysChem* **2010**, *11*, 1496−1504.
(153) Bruix, A.; Migani, A.; Vayssilov, G. N.; Neyman, K. M.; Libuda, J.; Illas, F. *Phys. Chem. Chem. Phys.* **2011**, *13*, 11384−11392.
(154) Negreiros, F. R.; Fabris, S. *J. Phys. Chem. C* **2014**, *118*, 21014−21020.
(155) Happel, M.; Mysliveček, J.; Johánek, V.; Dvořák, F.; Stetsovych, O.; Lykhach, Y.; Matolín, V.; Libuda, J. *J. Catal.* **2012**, *289*, 118−126.
(156) Ke, J.; Zhu, W.; Jiang, Y.; Si, R.; Wang, Y. J.; Li, S. C.; Jin, C.; Liu, H.; Song, W. G.; Yan, C. H.; Zhang, Y. W. *ACS Catal.* **2015**, *5*, 5164−5173.
(157) Zafiris, G. S.; Gorte, R. J. *J. Catal.* **1993**, *143*, 86−91.
(158) Smirnov, M. Y.; Graham, G. W. *Catal. Lett.* **2001**, *72*, 39−44.
(159) Škoda, M.; Cabala, M.; Matolinova, I.; Prince, K. C.; Skála, T.; Šutara, F.; Veltruska, K.; Matolín, V. *J. Chem. Phys.* **2009**, *130*, 034703−034709.
(160) Skála, T.; Šutara, F.; Škoda, M.; Prince, K. C.; Matolín, V. *J. Phys.: Condens. Matter* **2009**, *21*, 055005−055013.
(161) Men, Y.; Gnaser, H.; Zapf, R.; Hessel, V.; Ziegler, C.; Kolb, G. *Appl. Catal., A* **2004**, *277*, 83−90.
(162) Men, Y.; Gnaser, H.; Zapf, R.; Hessel, V.; Ziegler, C. *Catal. Commun.* **2004**, *5*, 671−675.
(163) Varga, E.; Pusztai, P.; Óvári, L.; Oszkó, A.; Erdőhelyi, A.; Papp, C.; Steinrück, H. P.; Kónya, Z.; Kiss, J. *Phys. Chem. Chem. Phys.* **2015**, *17*, 27154−27166.
(164) Ševčíková, K.; Kolářová, T.; Skála, T.; Tsud, N.; Václavů, M.; Lykhach, Y.; Matolín, V.; Nehasil, V. *Appl. Surf. Sci.* **2015**, *332*, 747−755.
(165) Salazar-Villalpando, M. D.; Berry, D. A.; Cugini, A. *Int. J. Hydrogen Energy* **2010**, *35*, 1998−2003.
(166) Hu, S.; Wang, W.; Wang, Y.; Xu, Q.; Zhu, J. *J. Phys. Chem. C* **2015**, *119*, 18257−18266.
(167) Chen, S.; Li, L.; Hu, W.; Huang, X.; Li, Q.; Xu, Y.; Zuo, Y.; Li, G. *ACS Appl. Mater. Interfaces* **2015**, *7*, 22999−23007.
(168) Martin, D.; Duprez, D. *J. Phys. Chem.* **1996**, *100*, 9429−9438.
(169) Ono, L. K.; Behafarid, F.; Cuenya, B. R. *ACS Nano* **2013**, *7*, 10327−10334.
(170) Chen, H. Y. T.; Tosoni, S.; Pacchioni, G. *J. Phys. Chem. C* **2015**, *119*, 10856−10868.
(171) Tosoni, S.; Chen, H. Y. T.; Pacchioni, G. *Surf. Sci.* **2016**, *646*, 230−238.
(172) Vecchietti, J.; Bonivardi, A.; Xu, W.; Stacchiola, D.; Delgado, J. J.; Calatayud, M.; Collins, S. E. *ACS Catal.* **2014**, *4*, 2088−2096.
(173) Yang, J. J.; Strachan, J. P.; Miao, F.; Zhang, M.-X.; Pickett, M. D.; Yi, W.; Ohlberg, D. A. A.; Medeiros-Ribeiro, G.; Williams, R. S. *Appl. Phys. A: Mater. Sci. Process.* **2011**, *102*, 785−789.

DOI: 10.1021/acscatal.7b01913
ACS Catal. 2017, 7, 6493−6513